J. Fluid Mech. (2013), *vol.* 735, *pp.* 203–248. © Cambridge University Press 2013
doi:10.1017/jfm.2013.498

On the highest non-breaking wave in a group: fully nonlinear water wave breathers versus weakly nonlinear theory

Alexey V. Slunyaev[1,2,3,†] **and Victor I. Shrira**[1]

[1]Department of Mathematics, EPSAM, Keele University, Keele ST5 5BG, UK

[2]Department of Nonlinear Geophysical Processes, Institute of Applied Physics, 46 Ulyanova Street, N. Novgorod 603950, Russia

[3]Nizhny Novgorod State Technical University, 24 Minina Street, N. Novgorod 603950, Russia

(Received 11 March 2013; revised 10 September 2013; accepted 13 September 2013; first published online 23 October 2013)

In nature, water waves usually propagate in groups and the open question about the characteristics of the highest possible wave in a group is of significant theoretical and practical interest. We examine the problem of the highest non-breaking wave in a wave group by direct numerical simulations of the exact Euler equations. The main aim of the study is twofold: (i) to describe the highest wave in a group in fully nonlinear setting and find its dependence on parameters; (ii) to examine correspondence between the exact breather solutions of weakly nonlinear analytic theory based on the integrable nonlinear Schrödinger (NLS) equation and their strongly nonlinear analogues. In contrast to weakly nonlinear models the very notion of the highest wave is ill-defined: the maximal crest elevation, the maximal trough-to-crest height and the deepest trough all occur at close but different moments; correspondingly, we have to speak about distinctively different extreme waves. In the simulations small initial perturbation of a uniform wave train were prescribed in a way ensuring that the initial perturbation excites a single breather-type modulation. The ensuing growth results in higher wave magnitudes and takes longer time to develop compared with the NLS theory. The maxima of crest elevation noticeably exceed their weakly nonlinear analogues. The wave with the highest crest differs significantly from the unmodulated wave: the local wavelength contracts considerably, the crest becomes noticeably higher; the vicinity of the crest of such an extreme wave is close to that of the limiting Stokes periodic wave. Thus, the shape of the maximal crest wave is almost universal, i.e. it practically does not depend on the way the wave group evolved, or even whether there was initially more than one group. The evolution of a single NLS breather has been shown to have a qualitatively similar but quantitatively quite different analogue in the fully nonlinear setting. The one-to-one mapping of the NLS breather solutions onto fully nonlinear ones has been constructed. The fully nonlinear breathers are found to be robust, which provides grounds for applying the results for developing short-term deterministic forecasting of rogue waves.

Key words: nonlinear instability, solitary waves, surface gravity waves

† Email address for correspondence: Slunyaev@hydro.appl.sci-nnov.ru

https://doi.org/10.1017/jfm.2013.498 Published online by Cambridge University Press

1. Introduction

Anomalously high or rogue waves observed from time to time on the sea surface attract a lot of attention for understandable practical reasons (Nieto Borge 2001, 2005, 2009; Dysthe, Krogstad & Müller 2008; Kharif, Pelinovsky & Slunyaev 2009). It would be highly desirable to be able to predict extreme waves, to know in advance when and what kind of extreme wave one might expect. On the theoretical side the only known extreme wave characteristics are those of the highest steady uniform wave train, strictly potential and strictly two-dimensional: the Stokes' steady wave (Michell 1893; Longuet-Higgins 1975). Since it is also known that the Stokes wave trains are inherently unstable (e.g. Benjamin & Feir 1967; Longuet-Higgins 1978; McLean 1982), it is not obvious how, or even whether, the extreme waves in nature are somehow related to the highest steady wave. In this work we are making just a step aside from the Stokes wave certainty, we are concerned with the most basic question: if a given monochromatic uniform Stokes wave train is somehow slightly perturbed, what are the characteristics of the ensuing maximal possible wave. To get a meaningful answer to this deceptively simple naive question, which is the subject of this work, we first reformulate it in a more precise way.

The fact that the initially uniform wave trains are modulationally unstable and have a tendency to disintegrate into wave groups, with the highest wave in such groups being noticeably higher than the wave height in the original train, has been known since the mid-1960s (e.g. Lighthill 1965; Benjamin & Feir 1967). This modulational (or Benjamin–Feir (BF)) instability was intensively studied both theoretically and experimentally, see e.g. the review by Yuen & Lake (1982). It was also studied in the more general context of nonlinear waves of other physical nature and has found applications in many branches of science (see, e.g., the historical essay by Zakharov & Ostrovsky 2009). In recent years, water wave modulation was studied extensively as the likely mechanism leading to wave breaking and anomalous freak or rogue waves in the ocean (Song & Banner 2002; Kharif *et al.* 2009; Babanin 2011), Certainly, this nonlinear mechanism results not only in the increase of the magnitude of the maximal waves, but also affects the probability of such events (e.g. Janssen 2004; Onorato *et al.* 2009). However, in this study and in our overview we consider only deterministic wave dynamics.

The full Euler equations for water waves are too difficult to be exhaustively examined and the progress in the understanding of nonlinear wave field evolution was advanced by building and thoroughly studying a hierarchy of simplified models. The greatest clarity in understanding nonlinear wave dynamics was achieved within the framework of the nonlinear Schrödinger (NLS) equation, derived for unidirectional potential waves under the approximation of small but finite wave steepness and narrow-band spectrum (e.g. Zakharov 1968; Whitham 1974; Craik 1985; Newell 1985). This equation is exactly solvable, it can be integrated by means of the inverse scattering technique (IST), which effectively reduces solving the Cauchy problem for the NLS equation to the analysis of a linear boundary-value problem with variable coefficients called the scattering problem (e.g. Newell 1985; Drazin & Johnson 1996). This approach was discovered and became popular long after the BF instability had become known, it is a powerful tool for nonlinear wave analysis. According to the IST, in the generic case the NLS solutions are represented by two kinds of spectra of the associated linear scattering problem, the discrete and the continuous spectrum. The former plays a major role and corresponds to the so-called 'unstable' modes, manifesting themselves as localized nonlinear wave groups,

https://doi.org/10.1017/jfm.2013.498 Published online by Cambridge University Press

when either zero conditions at infinities or periodic conditions are satisfied. The spectrum of the associated scattering problem does not change in time. Therefore, the solutions corresponding to the time-independent spectra, i.e. envelope solitons or breathers, are eternal nonlinear elements of the wave fields, although the patterns themselves might be evolving. These elements hold an essential part of wave field energy and interact elastically among themselves and with all other constituents of the wave field. Within the NLS framework the knowledge of the spectrum of the associated scattering problem opens the possibility of deterministic forecasting of the wave dynamics, in particular, extreme events. Envelope solitons upon the uniform background are frequently called breathers due to their characteristic 'breathing' evolution. Each breather solution describes the process of modulational instability growth and subsequent wave evolution for a specific initial perturbation (e.g. Ablowitz & Herbst 1990; Osborne 2010; Shrira & Geogjaev 2010). Since the breathers interact in a simple well-known way they are the key basic elements for comprehending the entire wave dynamics within the NLS equation. A long but incomplete list of breather solutions can be found in Dysthe & Trulsen (1999); it was significantly enriched in recent years, mostly due to the discovery of higher-order rational solutions (e.g. Akhmediev, Ankiewicz & Soto-Crespo 2009; Dubard *et al.* 2010; Gaillard 2012).

Thus, within the NLS equation the entire picture of dynamics of modulationally unstable waves, or most of it, can be described in terms of interacting breathers. It is important to mention that the dynamics of modulationally unstable fields is sensitive to perturbations, since a small perturbation of the initial conditions might affect the IST spectrum; in particular, waves may start to evolve apparently chaotically, (see among others Lo & Mei 1985; Ablowitz & Herbst 1990; Ablowitz *et al.* 2001). There are numerous attempts of applying the IST to the analysis of laboratory and *in situ* measured intense waves (e.g. Islas & Schober 2005; Slunyaev 2006; Schober & Calini 2008; Osborne 2010). However, the full Euler equations are not integrable even for two-dimensional motions and it is not clear to what extent the NLS equation captures the evolution of real nonlinear wave fields. It is not clear to what extent the breather-like solutions survive in the full equations; an even bigger question stems from the fact that the interactions between the breather-like patterns are no longer elastic. One of the main aims of this paper is to examine relations between the NLS solutions and more realistic fully nonlinear waves governed by the two-dimensional potential Euler equations, with the main focus on the extreme non-breaking waves. More specifically, we will concentrate upon the evolution of a single breather, where a possibility of the one-to-one mapping is *a priori* the most likely.

Tanaka (1990) was the first to examine the question of what is the biggest wave the modulational instability can produce for a given uniform wave train. Introducing small initial sideband perturbations to the wave train, Tanaka (1990) simulated the evolution of wave trains in a periodic domain employing the fully nonlinear Dold & Peregrine numerical code (see the references in Henderson, Peregrine & Dold 1999), and compared results with the simulations of the NLS equation and available laboratory data. The initial uniform wave train was prescribed by the third-order Stokes wave with the initial perturbations chosen as sidebands of 10 % amplitude of the dominant wave. The perturbation wavelength was chosen to excite the most unstable mode. The initial wave steepness in the simulations was in the range 0.05–0.17. According to Tanaka (1990), the maximum amplification of the surface elevation attained by non-breaking waves, is $\sim$3.4, while for a breaking wave the maximal amplification is $\sim$3.7 (see figure 6 in Tanaka 1990). A rather good agreement between the NLS equation and the fully nonlinear simulations was reported (cf. figures 3 and 6 in Tanaka (1990)).

https://doi.org/10.1017/jfm.2013.498 Published online by Cambridge University Press

Henderson *et al.* (1999) performed a more detailed study using the same numerical code as Tanaka (1990); the initial condition was chosen to be a modulated wave train with n waves and m modulations, with n and m being integers. Similar to Tanaka (1990), the 10 % perturbation was introduced as a pair of sidebands to the carrier waves. A set of values of the initial wave steepness, number of waves in the prescribed modulation and various phase relations between the carrier wave harmonic and the perturbation harmonics were considered. The main result was delineation of breaking and non-breaking regimes of evolution for the chosen class of initial conditions. The results were summarized in a diagram in the parameter space of wave steepness versus number of waves in one modulation. No systematic study of the maximal wave enhancement was carried out by Henderson *et al.* (1999). Seemingly it slightly exceeds three for the first steep wave event (see their figure 12), although may be even larger at a later stage of the wave evolution. Strong dependence of the time and intensity of the wave enhancement on the phase relation between the dominant and perturbation modes was noticed. The maximal wave groups were compared with the breather solutions of the NLS equation and a rather good agreement was emphasized.

Note that the weakly nonlinear NLS theory predicts the maximum wave amplitude attainable by a single breather to be equal to three (e.g. Peregrine 1983; Dysthe & Trulsen 1999; Slunyaev 2006; Osborne 2010). The NLS equation also describes the maximal wave amplification and the time it takes for the wave to attain it by quite simple formulae depending on only one compound parameter, which is a combination of two physical parameters, the wave steepness and the number of waves in one modulation (see § 2 below). Thus, on the one hand, there is a reasonable agreement between the NLS equation and fully nonlinear simulations of pretty steep modulated waves, at least for the examples considered by Tanaka (1990) and Henderson *et al.* (1999); on the other hand, the NLS model provides a simple quantitative description of modulated wave evolution. However, it is not clear how to utilize the simplicity of the NLS solutions and reported similarity of behaviour of the NLS and full Euler solutions. First, to examine the similarity quantitatively it has to be ensured that the same initial conditions both for the NLS and full Euler equations apply. This is not the case in the simulations by Tanaka (1990) and Henderson *et al.* (1999). The NLS breather solution represents a single unstable nonlinear mode, while the initial conditions employed by Tanaka (1990) and Henderson *et al.* (1999) contain several unstable modes, although one of these modes is dominant. The behaviour of the system with several unstable modes might differ significantly from that of the single-mode system. There are also related important open questions concerned with robustness of the single-mode solutions. Within the NLS framework it is straightforward to analyse multimodal (multibreather) solutions; one can easily find the wave field for any time, however large. It is important to know the sensitivity of the Euler equations solutions to perturbations of initial conditions. In particular, the NLS equation predicts that it is the longest initial perturbations with the weakest growth rates which attain the highest amplitude, at present it is not known whether such perturbations will also attain the maximal amplitudes in the presence of much faster growing shorter perturbations. The present work addresses these open questions.

Since the breathers are the key basic elements of wave field evolution within the NLS framework and are expected to play a major role in the fully nonlinear setting as well, we build the map: the NLS breathers–their Euler equations counterparts. The solutions of the exact Euler equations are obtained by means of fully nonlinear numerical simulations. To ensure that the initial conditions for the simulations are as close as possible to those of the NLS breather the initial conditions were specified

https://doi.org/10.1017/jfm.2013.498 Published online by Cambridge University Press

as a 'numerically exact' Stokes wave train perturbed in accordance with the exact NLS breather. Thus, we are able to simulate the fully nonlinear analogue of the NLS breather, capturing the basic solution describing a single mode of the modulational instability. We trace evolution of such fully nonlinear breathers focusing on the extreme non-breaking waves. The notion of the wave of maximal amplitude is ill-defined in this context, hence, we examine three types of extreme waves characterized by, respectively, the highest crest, the deepest wave trough and the maximal trough-to-crest wave height. The wave with the highest crest is considered in detail, in particular, its surface elevation profile and the envelope are examined. The profile of the highest crest wave proved to be of nearly universal shape close to that of the highest Stokes wave with the corner at the crest. The wave train containing the highest crest wave consists of very steep waves and is very short, the standard notion of wave envelope becomes inapplicable.

The paper is organized as follows. A brief summary of relevant analytic results provided by the NLS equation, with the emphasis on the periodic-in-space NLS breathers, is given in § 2. Section 3 briefly describes the validation of the codes employed in this study and provides sample simulations which outline the general picture of evolution of a single fully nonlinear breather. The effects of imperfect initial conditions, numerical noise and strong nonlinearity on breather evolution are also briefly discussed. Appendix A provides a very brief description of the numerical codes, complemented in appendix B by a description of how the initial conditions for the simulations of the primitive water wave equations are specified. Section 4 summarizes the results of simulations covering a wide range of initial wave steepnesses and modulation lengths. In § 5 the profiles of the extreme waves and the wave envelope are considered in detail. Discussion of the robustness of the obtained results and the effects of interactions between two wave groups are the subject of § 6. We end the paper with a short section of concluding remarks, where the results are summarized and discussed from the perspective of short-term deterministic forecasting of rogue waves.

2. Breathers and the NLS weakly nonlinear framework

Evolution of weakly nonlinear unidirectional deep-water surface waves in the leading-order in nonlinearity is governed by the NLS equation (e.g. Whitham 1974; Craik 1985; Newell 1985)

$$\mathrm{i}\left(\frac{\partial q}{\partial t}+\frac{\omega_0}{2k_0}\frac{\partial q}{\partial x}\right)+\frac{\omega_0}{8k_0^2}\frac{\partial^2 q}{\partial x^2}+\frac{\omega_0 k_0^2}{2}|q|^2 q=0, \tag{2.1}$$

where the complex function $q(x,t)$ is the wave envelope amplitude, t is time and x is the spatial coordinate in the direction of wave propagation, k_0 is the carrier wavenumber, $\omega_0=\sqrt{gk_0}$ and g is the acceleration due to gravity. In the standard non-dimensional form the NLS equation reads

$$\mathrm{i}\frac{\partial Q}{\partial T}+\frac{\partial^2 Q}{\partial X^2}+2|Q|^2 Q=0, \tag{2.2a}$$

where

$$X=2k_0\left(x-C_g t\right),\quad T=\frac{\omega_0}{2}t,\quad Q=\frac{k_0}{\sqrt{2}}q,\quad C_g\equiv\frac{\omega_0}{2k_0}, \tag{2.2b}$$

https://doi.org/10.1017/jfm.2013.498 Published online by Cambridge University Press

C_g is the group speed of linear waves with wavenumber k_0 and frequency ω_0. Since the NLS equation admits scaling transformation of dependent and independent variables, it is often convenient to use alternative stretched non-dimensional variables employing characteristic wave steepness s_0,

$$X = \sqrt{2} s_0 k_0 \,(x - Ct)\,, \quad T = s_0^2 \frac{\omega_0}{4} t, \quad Q = \frac{k_0}{s_0} q. \tag{2.3}$$

The advantage of this coordinate stretching is that if a dimensional wave has steepness s_0, $s_0 \equiv k_0 a_0$, where $a_0 = |q|$ is the wave amplitude, then the non-dimensional wave will have unit amplitude. For our objectives this form of non-dimensionalization is more convenient.

The NLS equation is one of the first discovered exactly solvable equations (see Zakharov & Shabat 1972), wave evolution within its framework has been thoroughly studied for over four decades and is now well understood. The NLS equation (2.1) provides the conceptual framework for comprehending fully nonlinear waves. In this section we summarize the current understanding of the particular class of the NLS solutions, the breathers, as the fundamental elements of wave field nonlinear dynamics and the most likely prototypes of strongly nonlinear rogue waves.

In the dimensional NLS equation (2.1) the complex envelope amplitude, $q(x, t)$, specifies both the surface elevation, $\eta(x, t)$, and the velocity potential at the still water level, $\phi(x, t, z = 0)$,

$$\eta = \frac{1}{2}\left[q \exp(\mathrm{i}\omega_0 t - \mathrm{i}k_0 x) + \text{c.c.}\right], \quad \phi(z = 0) = \frac{\mathrm{i}}{2}\frac{\omega_0}{k_0}\left[q \exp(\mathrm{i}\omega_0 t - \mathrm{i}k_0 x) - \text{c.c.}\right]. \tag{2.4}$$

In this approximation the velocity potential at the surface, $\Phi(x, t) \equiv \phi(x, t, z = \eta)$ is $\Phi(x, t) \approx \phi(x, t, z = 0)$. Higher-order reconstruction formulae have to be used to express the physical fields in terms of the complex wave amplitude, $q(x, t)$, taking into account bound waves at multiple wavenumbers and the induced long-scale low-frequency motions (see, e.g., Slunyaev 2005; Trulsen 2006, and reference therein). This approach is used in § 6 for prescribing initial conditions for double rational breathers; the third-order asymptotic theory is employed. For steep waves the effects due to the bound waves are essential; this requires distinguishing between the wave steepness specified on the basis of the free wave component, $s_0 \equiv k_0 a_0$, and that obtained employing the wave height in x-space representation, $s \equiv k_0 H/2$.

The NLS equation possesses the similarity parameter characterizing the ratio of nonlinear and dispersion terms which we denote as R_{BF}. For a modulated wave train with the modulation wavenumber, K, it takes the form

$$R_{BF} \equiv 2\sqrt{2} s_0 N_w, \tag{2.5}$$

where $N_w \equiv k_0/K$ is the number of individual waves within one modulation in the space domain.

The exact solution of (2.1) in the form of a uniform wave, $q = a_0 \exp(\mathrm{i}a_0^2/2t)$ is unstable with respect to long perturbations due to the BF instability. The corresponding growth rate σ_{BF} is easy to find by the linear perturbation theory and express in terms of R_{BF}, it is known to be (e.g. Newell 1985)

$$\frac{\sigma_{BF}}{\omega_0} = \frac{s_0^2}{R_{BF}} \sqrt{1 - \frac{1}{R_{BF}^2}}. \tag{2.6}$$

https://doi.org/10.1017/jfm.2013.498 Published online by Cambridge University Press

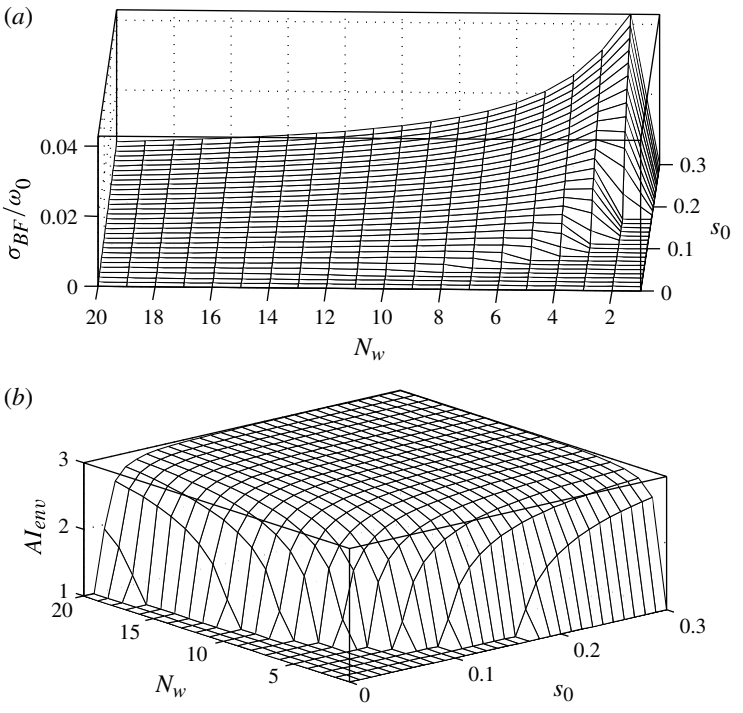


FIGURE 1. Modulational instability in the NLS framework: (*a*) the growth rate of the modulational instability; (*b*) the envelope amplitude maximal amplification, AI_{env}.

For any given modulation wavenumber K the instability occurs within the band $K < 2\sqrt{2}s_0k_0$. For a given modulation wavenumber K the BF instability starts on exceeding a threshold in steepness, the instability criterion can be expressed solely in terms of R_{BF}:$R_{BF} > 1$. In terms of modulation scale and unperturbed wave steepness: the given modulation grows when $N_w > 2^{-3/2}s_0^{-1}$. The unstable wave modulation manifests itself through growth of symmetrically located sidebands of the carrier wave, these sidebands grow by withdrawing energy from the dominant component as the instability develops.

The maximal growth rate σ_{BFmax} and the corresponding most unstable scale N_w are

$$\frac{\sigma_{BFmax}}{\omega_0} = \frac{s_0^2}{2} \quad \text{and} \quad N_{BFmax} = \frac{1}{2s_0}. \tag{2.7}$$

The growth rate σ_{BF} as a function of steepness and modulation length (the number of waves in one modulation) is plotted in figure 1(*a*). Note that for moderately steep waves of steepness $s_0 = 0.1$ the wave group resulting from the most unstable perturbations consists of only five waves.

An alternative description of the modulational instability in terms of nonlinear unstable modes is possible via the IST (see Drazin & Johnson 1996; Osborne 2010). Each unstable mode corresponds to an eigenvalue, λ, of the associated scattering problem. Such a mode corresponds to a breather solution of the NLS equation representing an oscillating wave packet on the background of a plane wave.

https://doi.org/10.1017/jfm.2013.498 Published online by Cambridge University Press

The most general breather solution in non-dimensional variables is (e.g. Slunyaev 2006)

$$Q(X,T)=\mathrm{e}^{2\mathrm{i}T}\frac{\cos\mu\cos(2\gamma(X-vT)+2\mathrm{i}\psi)-\cosh\psi\cosh(2\Gamma(X-VT)+2\mathrm{i}\mu)}{\cos\mu\cos(2\gamma(X-vT))-\cosh\psi\cosh(2\Gamma(X-VT))}, \tag{2.8a}$$

$$\Gamma=-\sinh\psi\cos\mu,\quad \gamma=\cosh\psi\sin\mu, \tag{2.8b}$$

$$V=-\frac{\cosh 2\psi\sin 2\mu}{\sinh\psi\cos\mu},\quad v=\frac{\sinh 2\psi\cos 2\mu}{\cosh\psi\sin\mu}, \tag{2.8c}$$

$$\lambda=\cos(\mu+\mathrm{i}\psi), \tag{2.9}$$

which generalizes the classical Peregrine, Kuznetsov–Ma and Akhmediev solutions we discuss below.

The Kuznetsov–Ma breathers correspond to $\lambda>1$ and are periodic in time (Kuznetsov 1977; Dysthe & Trulsen 1999); they cannot grow out of an infinitesimal perturbation of a plane wave. The Peregrine soliton occurs when $\lambda=1$ (Peregrine 1983) and is not periodic either in time or space. When $\lambda<1$, (2.8) describes the periodic in space Akhmediev breathers. These periodic in space but not in time breather solutions (2.8) can be written in a simpler form (Akhmediev, Eleonskii & Kulagin 1987)

$$Q(X,T)=\mathrm{e}^{2\mathrm{i}T}\frac{\lambda\cos 2\gamma X-\cosh(\sigma T-2\mathrm{i}\mu)}{\lambda\cos 2\gamma X-\cosh\sigma T}, \tag{2.10}$$

$$\gamma=\sqrt{1-\lambda^2},\quad \sigma=4\lambda\sqrt{1-\lambda^2},\quad \lambda=\cos\mu. \tag{2.11}$$

These solutions describe the growth of sideband perturbations of the plane wave (Ablowitz & Herbst 1990; Henderson *et al.* 1999). Their spatial period is $L=\pi/\gamma$, and hence the perturbation length and the breather eigenvalue, λ, are tightly linked. This results in the following elegant relation between R_{BF}, the integral parameter specified by (2.5), and the eigenvalue of the associated scattering problem (Osborne 2010)

$$\lambda=\sqrt{1-\frac{1}{R_{BF}^2}}. \tag{2.12}$$

The maximal amplification of the wave envelope is given by another remarkably simple formula,

$$AI_{env}\equiv\frac{\max_t\max_x|q(x,t)|}{\min_t\max_x|q(x,t)|}=1+2\lambda. \tag{2.13}$$

The maximum of the envelope amplification index AI_{env} equal to three occurs at $\lambda=1$. A plot of AI_{env} as function of the number of modulated waves, N_w, and the wave steepness, s_0, is shown in figure 1(*b*). The most linearly unstable perturbation corresponds to $\lambda=2^{-1/2}$ and results in $AI_{env}\approx 2.4$. This breather is plotted in figure 2(*a*); it has maximum amplitude at $T=0$ and tends to the plane unperturbed wave with unit amplitude as $T\to\pm\infty$. If $1/2\leqslant\lambda\leqslant 1$, the envelope, as in the example illustrated in figure 2(*a*), touches the zero level at $T=0$ at points $\pm X_0$,

$$X_0=\frac{1}{2\sqrt{1-\lambda^2}}\arccos\frac{2\lambda^2-1}{\lambda}. \tag{2.14}$$

https://doi.org/10.1017/jfm.2013.498 Published online by Cambridge University Press

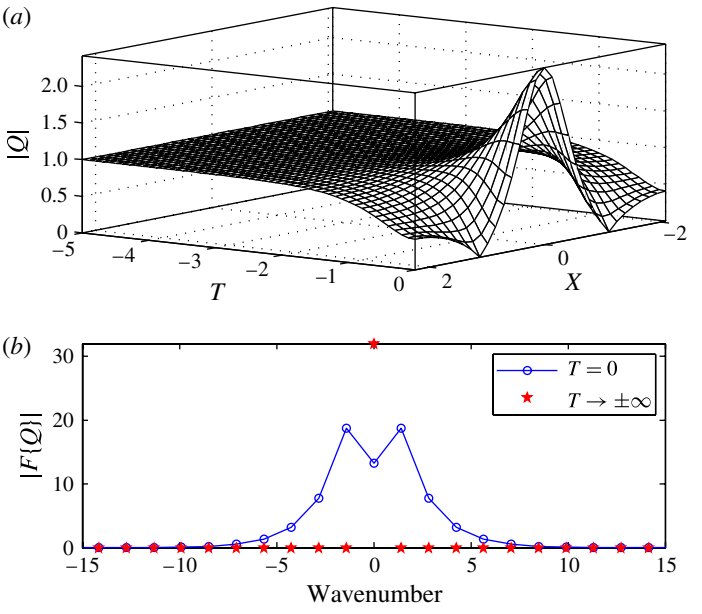


FIGURE 2. (Colour online) The periodic in space Akhmediev breather for $\lambda = 2^{-1/2}$: (*a*) the evolution of $|Q(X, T)|$; (*b*) scaled Fourier spectrum at the moment of maximum breather amplitude $T = 0$ (circles with line) and at $T \to \pm\infty$ (stars).

For the range $0 < \lambda < 1/2$ the breather envelope $|Q(X, T)|$ does not vanish anywhere. Note that for $0 < \lambda < 1/2$ the rogue wave criterion in the form $AI_{env} > 2$ cannot be fulfilled either.

Initially the Akhmediev breathers grow exponentially due to the energy transfer from the carrier wave to satellites. At the focusing time $T = 0$ the wave modulation peaks and then relaxes. The initial uniform plane wave is restored as $T \to \infty$. In figure 2(*b*) the Fourier spectrum for the wave train with infinitesimal perturbation is shown by stars, and the spectrum at the moment of maximal envelope focusing is given by circles connected by solid lines.

The lifetime of a rogue wave is one of the basic characteristics of these extreme events. It may be found for any chosen threshold level of envelope amplitude amplification, AI_{thr}, using the known analytic solution (2.10)

$$T_{life} = \frac{1}{2\lambda\sqrt{1-\lambda^2}}\cosh^{-1}\left[1 + \frac{1-\lambda}{1+AI_{thr}}\left(AI_{env}^2 - AI_{thr}^2\right)\right], \quad AI_{env} = 1 + 2\lambda. \tag{2.15}$$

The commonly used definition of rogue waves is based upon $AI_{thr} = 2$. Correspondingly, for the duration T_{life} the amplitude of the breather envelope exceeds threshold value AI_{thr} times the amplitude of the unperturbed wave, $|Q(X, T \to -\infty)|$. Formula (2.15) has solutions only for $(AI_{thr} - 1)/2 < \lambda \leqslant 1$. For $\lambda < (AI_{thr} - 1)/2$ the amplified wave does not exceed the threshold value. For the rogue wave specified by $AI \geqslant 2$ to emerge from an infinitesimal perturbation the eigenvalue λ should be within the range $1/2 < \lambda \leqslant 1$; then the envelope touches the zero level at some points, see (2.14).

In the linear limit, that is when the cubic term in the NLS equation (2.2) is strictly zero and the equation becomes a linear parabolic equation, the Gaussian

https://doi.org/10.1017/jfm.2013.498 Published online by Cambridge University Press

modulated wave group is an exact analytic solution. Its amplitude A_G decays with time as $A_G(t) = A_{G0}(1 + 16T^2/L_{G0}^4)^{-1/4}$, $A_{G0} \equiv A_G(t = 0)$ and spreads in space as $L_G/L_{G0} = (1 + 16T^2/L_{G0}^4)^{1/2}$, where L_G is the characteristic half-width of the packet, and $L_{G0} \equiv L_G(t = 0)$ (e.g. Slunyaev *et al.* 2002). Then a Gaussian group with an initial amplitude A_{G0} disperses and its amplitude A_G decreases. An *a priori* prescribed value of A_G is attained at time T_G

$$T_G = \frac{L_{G0}^2}{4}\sqrt{\left(\frac{A_{G0}}{A_G}\right)^4 - 1}. \tag{2.16}$$

To compare the lifetime of a breather with that of a transient Gaussian wave group, we relate their parameters in the following way: we set the initial amplitude of the Gaussian packet to be equal to the maximal amplitude of the breather $A_{G0} = 1 + 2\lambda$, and we equate the characteristic width of the packet to the distance from the maximum to zero $L_{G0} = X_0$. The breathers have initially unit amplitude and model rogue waves when the amplitude exceeds the value of 2, according to the adopted rogue wave definition $AI_{env} > 2$. Therefore, we put $A_G = 2$ in formula (2.16), and then the lifetime for the Gaussian rogue wave may be estimated as

$$T_{life}^G = \frac{L_{G0}^2}{2}\sqrt{\left(\frac{1 + 2\lambda}{2}\right)^4 - 1}, \quad \lambda \geqslant 1/2. \tag{2.17}$$

Lifetimes T_{life} and T_{life}^G as functions of λ behave in a similar fashion and result in similar values. They are non-zero for $\lambda > 1/2$ and grow monotonically with λ. In the limiting case of the Peregrine breather, $\lambda = 1$, $A_G = 2$, $A_{G0} = 3$, $L_{G0} = \sqrt{3}/2$, the lifetime T_{life} tends to $\sqrt{15}/6 \approx 0.65$ and T_{life}^G tends to $3\sqrt{65}/32 \approx 0.76$. Thus, there is no significant difference in the lifetimes of the NLS breathers and the linear Gaussian groups.

Introduce the direct Fourier transform with respect to x as

$$\hat{F}\{Q\} \equiv \int_0^{\pi/\gamma} Q \exp(\mathrm{i}kx)\,\mathrm{d}x, \tag{2.18}$$

where the integration is taken over the period of the solution, which is π/γ, see (2.8) and (2.10), and k is a discrete index, $k = 2\gamma j$, j is an integer. The inverse transform is given by the infinite summation over indices k. For the zero wavenumber $k = 0$, equation (2.18) gives the 'mass' integral of the solution, $F\{Q\}_{k=0} = \int_0^{\pi/\gamma} Q\,\mathrm{d}x$. Then the Fourier spectrum $\hat{F}\{Q\}$ for the Akhmediev solution (2.10) ($\lambda < 1$) reads (see Akhmediev & Ankiewicz 1997; Slunyaev 2010),

$$\hat{F}\{Q\} = \mathrm{e}^{2\mathrm{i}T}\left[M - 2\pi B\mathrm{e}^{\mathrm{i}\theta}\right], \tag{2.19a}$$

$$M = \frac{\pi}{\sqrt{1-\lambda^2}}\delta_k, \quad \theta = \arctan\left(\frac{\lambda}{\sqrt{1-\lambda^2}}\tanh 4T\lambda\sqrt{1-\lambda^2}\right), \tag{2.19b}$$

$$B_{k\neq 0} = \left(p - \sqrt{p^2-1}\right)^{-|k|/(2\sqrt{1-\lambda^2})}, \quad p = \frac{1}{\lambda}\cosh 4T\lambda\sqrt{1-\lambda^2}, \tag{2.19c}$$

where δ_k is the Kronecker symbol. It is significant that $|k|/(2\sqrt{1-\lambda^2}) = |j|$. Note that for each unstable mode a number of spectral satellites builds up along with the main harmonics. The contributions to the dominant wave component and the sidebands are readily separated in (2.19). It is easy to see that all of the sidebands are always in

https://doi.org/10.1017/jfm.2013.498 Published online by Cambridge University Press

phase with each other, but in the counterphase with the carrier wave when $T = 0$. The spectrum tail in (2.19) decays exponentially as a function of $|k|$.

For $T \to \pm\infty$ solution (2.10) tends to the plane wave with a specific phase shift,

$$Q \to \mathrm{e}^{2\mathrm{i}T}\mathrm{e}^{\mp 2\mathrm{i}\mu} \quad \text{as } T \to \pm\infty. \tag{2.20}$$

and, hence,

$$\hat{F}\{Q\}_{k=0} \to \frac{\pi}{\sqrt{1-\lambda^2}}\mathrm{e}^{2\mathrm{i}T}\mathrm{e}^{\mp 2\mathrm{i}\mu} \quad \text{as } T \to \pm\infty. \tag{2.21}$$

This property may also be obtained directly from (2.19), then $\theta = \mp(\mu - \pi/2)$ for $T \to \pm\infty$. In the limiting case of the Peregrine breather $\lambda = 1$: $\theta = \pm\pi/2$ as $T \to \pm\infty$.

For $k \neq 0$, solution (2.19) can be inverted, which yields

$$T = \frac{1}{4\lambda\sqrt{1-\lambda^2}}\cosh^{-1}\left[\frac{\lambda}{2}\left(B_k^{2\sqrt{1-\lambda^2}/|k|} + B_k^{-2\sqrt{1-\lambda^2}/|k|}\right)\right]. \tag{2.22}$$

It follows from (2.19) and (2.22), that in the limit $T \to -\infty$

$$\hat{F}\{Q\}_{k=0} \cong -\frac{\pi}{\sqrt{1-\lambda^2}}\mathrm{e}^{2\mathrm{i}T}\mathrm{e}^{2\mathrm{i}\theta} \quad \text{and} \quad \hat{F}\{Q\}_{k\neq 0} = -2\pi B_k \mathrm{e}^{2\mathrm{i}T}\mathrm{e}^{\mathrm{i}\theta}, \tag{2.23}$$

where θ is function of T and λ specified by (2.19). The ratio of two equalities in (2.23) provides the sideband harmonic Fourier amplitudes normalized by the zero-harmonic amplitude, which reads

$$B_k \cong \frac{\hat{F}\{Q\}_k}{\hat{F}\{Q\}_{k=0}}\frac{\mathrm{e}^{\mathrm{i}\theta}}{2\sqrt{1-\lambda^2}}. \tag{2.24}$$

Let us introduce a normalized amplitude of kth Fourier harmonic of perturbation Δ_k:

$$\Delta_k = 2\frac{|\hat{F}\{Q\}_k|}{|\hat{F}\{Q\}_{k=0}|}. \tag{2.25}$$

Then, the quantity $|B_k|$ in (2.22) may be estimated using (2.24), which gives the focusing time associated with the perturbation Δ_K in the original physical variables $k_0 K \equiv |k_0 - k|$, as

$$T_f \cong \frac{1}{4\lambda\sqrt{1-\lambda^2}}\cosh^{-1}\left[\frac{\lambda}{2}\left(\frac{\Delta_K}{4\sqrt{1-\lambda^2}}\right)^{2(\sqrt{1-\lambda^2}/K)} + \frac{\lambda}{2}\left(\frac{\Delta_K}{4\sqrt{1-\lambda^2}}\right)^{-2(\sqrt{1-\lambda^2}/K)}\right]. \tag{2.26}$$

Note that Δ_K is an appropriately normalized wave amplitude perturbation, for example, $\Delta_K = 0.01$ corresponds to a perturbation of the surface elevation with length $2\pi/K$ and the amplitude equal to 1 % of the unperturbed carrier wave. The modulation with length of the breather solution, L, corresponds to $K = 2\gamma$. The amplitude of the most energetic perturbation will be denoted hereinafter omitting the subscript, i.e. as Δ. The time when the breather with primordial perturbation level characterized by Δ attains the maximum modulation is denoted as T_f and hereinafter is referred to as the 'focusing time'. The expression for the focusing time T_f given by (2.26) may be

https://doi.org/10.1017/jfm.2013.498 Published online by Cambridge University Press

rewritten in terms of the R_{BF} and wave steepness. The inverse of the focusing time behaves similar to σ_{BF} shown in figure 1. In the context of the present study it is important to stress that the most unstable perturbation does not coincide with that with the maximal wave amplification.

The characteristic non-dimensional 'nonlinear time' $T_f = s_0^{-2}\omega_0 t_f$, where t_f is the dimensional focusing time, is estimated for the perturbation for the most unstable mode and $\Delta = 0.01$; it is found to be of order $O(10^1)$. For small perturbation level Δ the focusing time strongly depends on Δ; larger perturbations result in exponentially shorter focusing time. In this study the initial perturbation level is quite small, $\Delta = 0.01$; it is kept the same for all simulations.

The evolution of modulated waves with various phases between the carrier and the sidebands was examined by Henderson *et al.* (1999). It was found that the breather solution corresponds to the case when the modulational instability develops most slowly. Tanaka (1990) reports that the phase variation does not lead to a noticeable change in the wave enhancement magnitude except for some particular values of the phase. In contrast, Henderson *et al.* (1999) show that when the phase departs from the value prescribed by the breather exact solution, the wave enhancement decreases.

According to the Fourier presentation of the breather solution (2.19) and (2.24) the phases and amplitudes of harmonics are time dependent. We can say that particular values of phases are rigidly linked to particular values of amplitudes. However, there is an initially prescribed mismatch of the phases; this means that the sideband perturbation cannot be described by a single unstable breather mode, other unstable modes become excited as well. Then the process becomes more complicated, as several different unstable modes grow with different rates, withdrawing energy from the dominant wave and interacting with each other. In this study we focus on the situations where only a single mode is excited and consider excitation of other unstable modes as an undesirable parasitic effect. The NLS equation also admits exact solutions enabling one to describe simultaneous growth of any number of nonlinear modes. An example of a two-mode instability process resulting in emergence of a rational breather of second order is briefly discussed in § 6.

Formulae (2.12), (2.13), (2.15) and (2.26) are the key analytic formulae which allow description of the modulational instability in terms of breather solutions in the weakly nonlinear NLS consideration. Their predictions will be used in the study as the reference for the wave amplification, the focusing time and the lifetime of rogue-wave-type events.

3. Validation of the approach and examples

This study is based on direct numerical simulation of the potential Euler equations for planar deep-water gravity waves. The majority of simulations is conducted within the framework of the potential Euler equations in conformal variables (Zakharov, Dyachenko & Vasilyev 2002) without any simplifications; some simulations are repeated employing the high-order spectral method (HOSM), which resolves up to seven-wave interactions (West *et al.* 1987). Both codes are pseudospectral in the x domain. A few examples were modelled within the framework of the NLS equation integrated with the help of the split-step Fourier method (Lo & Mei 1985). A brief description of the numerical approaches is given in appendix A.

An important aspect of the present paper concerned with the setting of initial conditions is detailed in appendix B. The initial conditions employed in the present study for excitation of a single mode of modulational instability differ from those

https://doi.org/10.1017/jfm.2013.498 Published online by Cambridge University Press

conventionally used to initiate the growth of sidebands of wave trains (in particular, in Tanaka 1990; Henderson *et al.* 1999). The specific differences are:

(i) many coherent sidebands to the dominant wave are accurately prescribed; Stokes wave phase-locked components are modulated accordingly;

(ii) specific phase shift between the dominant harmonic and the perturbation is prescribed according to the explicit breather solution of the NLS equation.

Leaving aside the discussion of how realistic is the long-time dynamics as captured by exact solutions of the NLS equation, we first examine how the numerical noise, which always exists along with weak perturbations, may affect the numerical simulation of the breather solution. From the methodological perspective we discuss two examples of fully nonlinear simulations afterwards.

3.1. *NLS equation: simulation of the elevation evolution*

First, the exact breather solution is reproduced by means of the numerical solution of the NLS equation for the range of parameters considered in the study: $s_0 = 0.1$–0.15 and $N_w = 2$–20. The initial condition is specified by the complex envelope function $q(x, t = -t_f)$ provided by (2.10). These simulations, which we do not illustrate here, confirm the ability of the numerical code to reproduce the breather analytic solution almost perfectly for the cases concerned, including the essentially nonlinear stage, when the maximum modulation occurs. On the other hand, some time after the focusing moment, a deviation of the numerical solution from the analytic one becomes apparent. New unstable modes become excited and give rise to new wave oscillations. This effect has been observed many times in simulations of the NLS equation and its generalizations (see, for example, Lo & Mei 1985) and may be due to perturbation of the model, inappropriate discretization and also numerical noise (e.g. Ablowitz & Herbst 1990; Ablowitz *et al.* 2001).

Another series of simulations of the NLS equation (2.2) employed the initial condition in the form of surface elevation, $\eta(x, t = -t_f)$, of the weakly modulated Stokes wave train as described in appendix B. The best fit between the fully nonlinear wave shape $\eta(x, t = -t_f)$ and the real part of weakly nonlinear weakly modulated third-order solution for the sought-for complex amplitude function $q(x, t = -t_f)$ is found by virtue of an iterative procedure. Function q corresponds to the free wave component; the reconstruction formulas used to obtain the surface elevation are the same as used for the Dysthe equation, see Trulsen (2006). They take into account the second and third wave harmonics, and also the long-scale induced current. This procedure introduces a somewhat higher level of perturbations compared with the case considered above due to the approximation of the fully nonlinear solution by a weakly nonlinear analogue.

Figure 3 reports the simulation of the case $s_0 = 0.09$, $N_w = 9$ and $\Delta = 0.01$. The results are qualitatively similar to those discussed in the previous paragraph. The first wave 'breath' is very well reproduced, see the wave amplification in figure 3(*a*). The points of numerical data are distributed irregularly in time, they are most dense near the focusing moment and agree with the analytic curve. The spectrum of the most amplified wave in figure 3(*b*) shows excellent agreement during the first breath. At long scales there are some larger spectral amplitudes in figure 3(*b*), because the surface elevation is obtained from the complex amplitudes, q, employing the reconstruction formulae (2.4), which in the case of a rather wide spectrum of the envelope results in overlapping of complex conjugated parts, q and q^*.

https://doi.org/10.1017/jfm.2013.498 Published online by Cambridge University Press

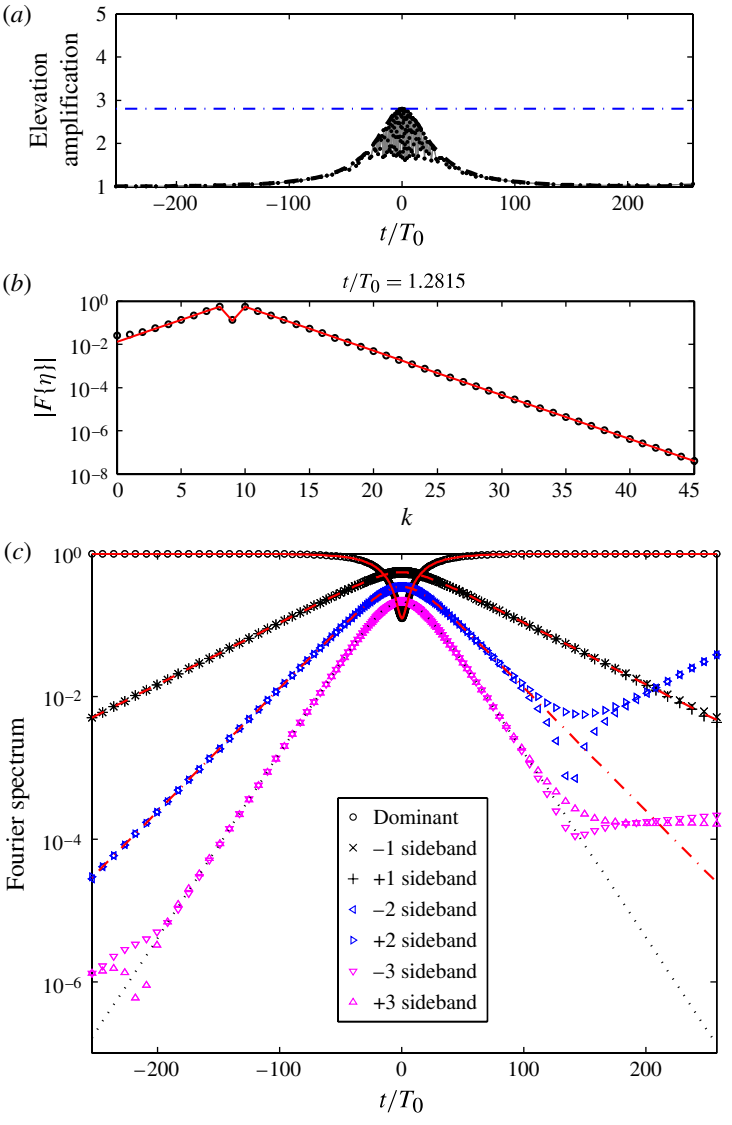


FIGURE 3. (Colour online) Simulation of the breather solution ($s_0 = 0.09$, $N_w = 9$, $\Delta = 0.01$) within the framework of the NLS equation. (*a*) Time dependence of the envelope amplification, AI_{env}: the thick dashed curve shows the analytic solution (2.13), points connected by grey lines correspond to the numerical simulation. The horizontal dash-dot line corresponds to the value $1+2\lambda$. (*b*) Scaled Fourier spectrum for the elevation (circles), and the analytic breather solution (solid line) for the moment of maximal amplification. (*c*) Evolution of scaled Fourier amplitudes of different wavenumbers on semilogarithmic scales: dominant (N_w) and sidebands, see the legend. Curves give the analytic solution, symbols represent the result of simulations.

Figure 3(*c*) displays the evolution of most energetic spectral components on a semilogarithmic scale. The dominant wave passes its energy to the satellites. The first pair of satellites, $k = N_w \pm 1$, is the most energetic. Again the numerical results, given by the symbols, agree very well with the analytic solution for the first wave breath,

https://doi.org/10.1017/jfm.2013.498 Published online by Cambridge University Press

in spite of some error in the initial condition for harmonics $N_w \pm 3$ clearly seen from figure 3(*c*). Later on the wave does not fully return to the initial state, other sidebands start to grow, which will give birth to other breathers later.

For very long simulations the errors accumulate into a noticeable deviation of simulations from the analytic description. It first becomes apparent due to the difference in the moment of maximum amplification, and then due to different amplification factors and the emergence of other unstable modes. We confine our interest to a moderate maximal number of waves in one modulation, $N_w \leqslant 20$; the larger numbers are most likely to be unrealistic.

3.2. *Examples of breather focusing within the Euler equations framework*

An example of the evolution of a breather within fully nonlinear simulations with the initial parameters $s = 0.05$, $N_w = 9$ and $\Delta = 0.01$, where it looks similar to that described by the NLS solution, is shown in figure 4. The main discrepancy is in the delay of focusing clearly seen from figure 4(*a*), while the maximum amplification attained by the breather is very close to the value provided by the analytic solution (2.13). At the instant of maximal amplification the wave shape somewhat differs from the NLS solution; see the corresponding Fourier spectrum in figure 4(*b*), where symbols show the result of the simulation at the moment of the most amplified surface elevation ($t \approx 111T_0$), while the lines show the analytic solution taken at the moment $t = 0$ when it is most amplified. The spectral tails of the simulated breather are skewed. It follows from figures 4(*b*) and 4(*d*), that in general the low-frequency sidebands have smaller amplitudes, although close to the moment of focusing the sideband $k = N_w - 1$ has larger amplitude than $k = N_w + 1$.

In the fully nonlinear case the focusing is delayed compared with the NLS equation, we assume that the effect of recurrence still takes place. Therefore, we compare in figure 4(*c*) the NLS solution at time instant $t = t_f$ (the solid lines), and the fully nonlinear solution at the moment $t \approx t_f + 2 \cdot 111T_0$ (circles). Within the NLS framework the spectrum at $t = t_f$ in figure 4(*c*) exactly coincides with the spectrum at the initial instant, $t = -t_f$. If in the fully nonlinear framework there was a perfect recurrence, the spectrum at $t \approx t_f + 2 \cdot 111T_0$ would coincide with the initial one and, thus, the circles would cover the lines in figure 4(*c*). In reality the recurrence is only approximate: after the stage of intensification the envelope perturbation almost returns to the initial state. The new unstable modes cannot be confidently discerned in the spectrum in figure 4(*c*). A closer analysis of the spectrum evolution reveals different dynamics of distant sidebands; in fact, new unstable modes are getting excited. Compared with the NLS solution the dominant wave releases less energy, see figure 4(*d*), but due to the bound harmonics components the wave amplification in figure 4(*a*) is very similar to that predicted by the NLS equation for the envelope.

Evolution of a steeper breather with initial parameters $s = 0.09$, $N_w = 9$ and $\Delta = 0.01$ is shown in figure 5. Note the much shorter focusing time compared with figure 4 and its significant increase compared with the NLS theory. The maximal wave amplification occurs in the simulation at $t \approx 35T_0$, (that is, 35 periods later than is predicted by the NLS equation); it is noticeably higher than the value of AI_{env}. At the moment of maximal focusing the wave becomes so steep and its crest so sharp that its spectrum tail decays slowly. The focused wave group is so short that the spectrum of the enveloping curve is also decaying slowly. As a result the Fourier spectrum of the modulated wave train is not of the comb-shaped type, compare figures 4(*b*) and 5(*b*). In figure 5(*b*) the spectral components corresponding to the second and higher harmonics of the carrier wave cannot be discerned. It follows

https://doi.org/10.1017/jfm.2013.498 Published online by Cambridge University Press

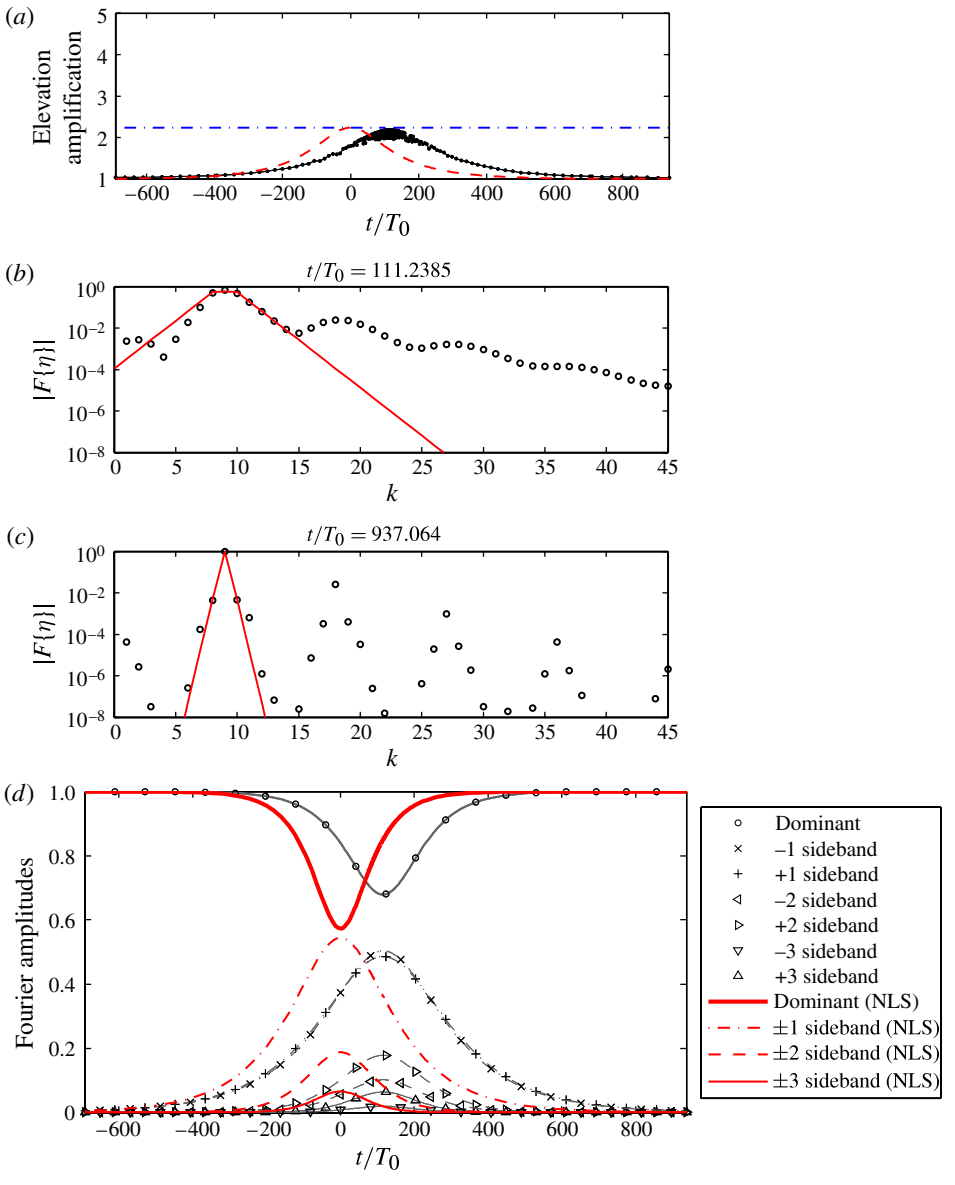


FIGURE 4. (Colour online) Simulation of the breather evolution ($s = 0.05$, $N_w = 9$, $\Delta = 0.01$) within the fully nonlinear framework. (*a*) Evolution of the wave crest amplification, AI_{cr}, is shown by points connected by lines. The dashed curve shows corresponding AI_{env} of the analytic breather solution, the horizontal dash-dot line shows the value $1 + 2\lambda$. (*b*) Scaled Fourier spectrum for the surface elevation at the moment of maximum amplification (circles), and the analytic solution of the NLS equation for $t = 0$ (solid line). (*c*) Similar to (*b*), but the simulated spectrum is shown for the instant $t \approx 937T_0$, and the analytic solution for $t \approx 692T_0$; see the discussion in the text. (*d*) Evolution of scaled Fourier amplitudes corresponding to different wavenumbers (see the legend). Curves give the analytic solution, and symbols over grey lines represent the results of simulations.

https://doi.org/10.1017/jfm.2013.498 Published online by Cambridge University Press

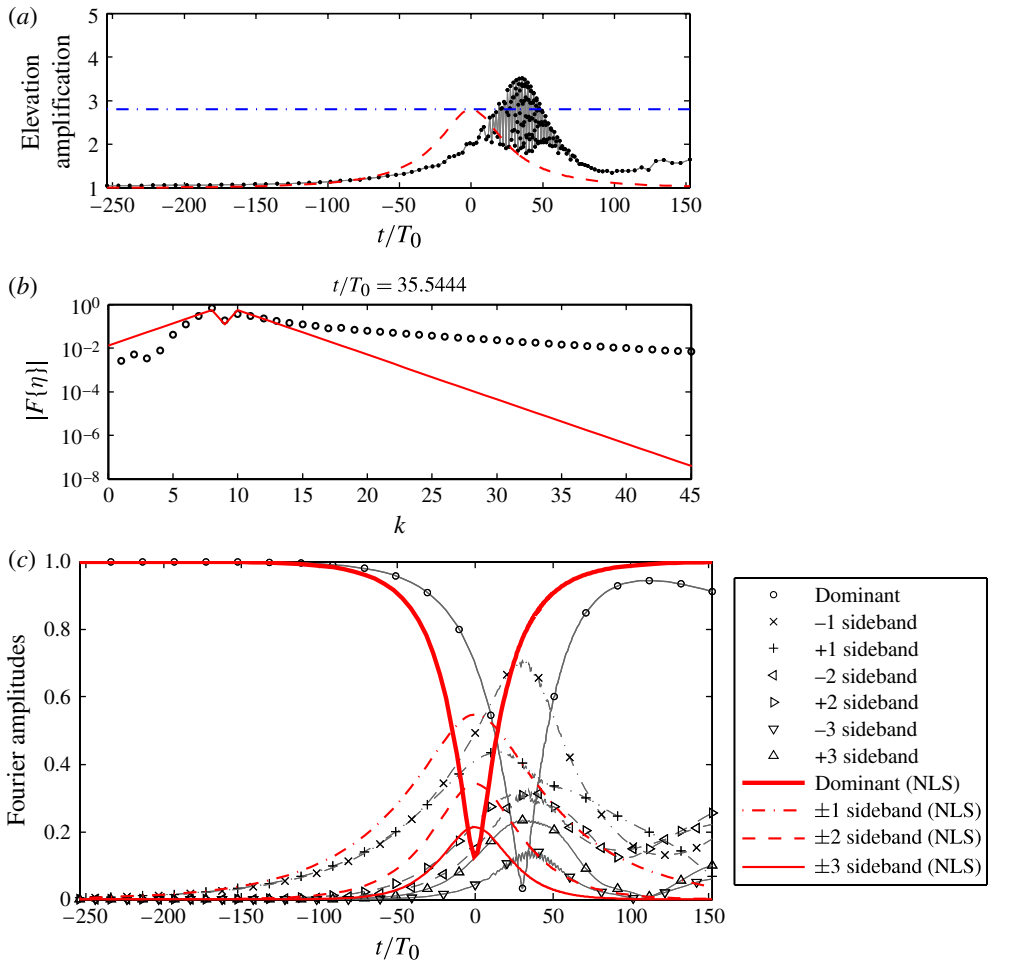


FIGURE 5. (Colour online) Simulation of the breather solution ($s = 0.09$, $N_w = 9$, $\Delta = 0.01$) within the fully nonlinear framework. (*a*) Evolution of the wave crest amplification AI_{cr} is depicted by points connected with lines. The dashed curve shows corresponding AI_{env} of the analytic breather solution, the horizontal dash-dot line shows the value $1 + 2\lambda$. (*b*) Scaled Fourier spectrum for the surface elevation at the moment of maximum amplification (circles), and the analytic breather solution for $t = 0$ (solid line). (*c*) Evolution of scaled Fourier amplitudes corresponding to different wavenumbers (see the legend). Curves give the analytic solution, while symbols over solid grey lines represent the result of simulations.

from figure 5(*c*) that in the course of the evolution, in contrast to the example with lesser steepness in figure 4, the dominant wave loses even more energy than in the weakly nonlinear theory. Also unexpectedly from a more detailed consideration of figure 5(*a*,*c*) it follows that the maximal wave elevation amplification is attained a few wave periods after the moment of the maximal withdrawal of energy from harmonic $k = N_w$. Although the low-wavenumber spectral tail generally has less energy than the high-wavenumber one, see figure 5(*b*), strong discrimination between sidebands $N_w \pm 1$ is observed in figure 5(*c*); the sideband $N_w - 1$ becomes for some time the most energetic spectral component. During this period one wave oscillation is lost in the

https://doi.org/10.1017/jfm.2013.498 Published online by Cambridge University Press

spatial domain similar to the observation by Henderson *et al.* (1999). The evolution of different sidebands in figure 5(*c*) is rather complicated, in particular, they attain their local maxima at different moments, which is likely to reduce the possible effect of nonlinear wave focusing. Emergence of other unstable modes is evident in the presented characteristic sample simulation. However, it should be noted that in the time interval we are primarily interested in, that is up to the formation of the first 'extreme wave', all other unstable modes are indiscernible.

Thus, we have verified that fully nonlinear counterparts of the NLS breathers exist and the employed numerical approaches do capture the evolution of a single breather within the fully nonlinear Euler equations with the desired accuracy. Individual histories of evolution allow a detailed comparison with the NLS breathers with the same initial conditions, which makes possible a detailed comparison between the two solutions and one-to-one mapping.

4. Breather evolution in fully nonlinear simulations

To build up a comprehensive picture of fully nonlinear evolution of breathers and scan the parameter space the simulations were performed for the initial steepness s sweeping the range 0.04–0.24 and for an integer number of waves in one modulation, $N_w = 2$–20. A limited number of runs have also been performed for rational numbers $N_w = n/m$, i.e. for n waves in m modulations. Since very intense short wave-groups break before they attain significant amplifications, we restrict our consideration to $N_w = 3, 7/2, 4, \ldots, 20$ and $s = 0.04$–0.16. The normalized magnitude of initial perturbation is always the same: $\Delta = 0.01$.

4.1. *Wave enhancement*

When there is a single growing wave group in the simulation domain the analysis of surface elevation fields is straightforward: the maximal elevation, the minimal elevation and their difference correspond respectively to the crest amplitude, trough amplitude and the trough-to-crest height of the corresponding extreme waves. In contrast to the weakly nonlinear framework, in order to capture essential aspects of wave dynamics near the peak of the group, we have to use at least several characteristics. We introduce a set of the following 'amplification indices' for: the wave crest elevation,

$$AI_{cr} \equiv \frac{\max_t \max_x \eta(x,t)}{\max_x \eta(x, t=-t_f)}, \tag{4.1}$$

the wave trough amplification,

$$AI_{tr} \equiv \frac{\min_t \min_x \eta(x,t)}{\min_x \eta(x, t=-t_f)}, \tag{4.2}$$

and the wave trough-to-crest height amplification,

$$AI_H \equiv \frac{\max_t (\max_x \eta(x,t) - \min_x \eta(x,t))}{\max_x \eta(x, t=-t_f) - \min_x \eta(x, t=-t_f)}. \tag{4.3}$$

In our study we make no distinction between up-crossing and down-crossing wave heights. Note that we consider wave evolution by looking at the spatial snapshots taken at various instants of time, but not the time series taken at a particular point.

We concentrate on the wave group nonlinear focusing and the maximal characteristics attained. The general picture of wave group focusing from this perspective in the course of breather dynamics is outlined in figures 6–10. For

https://doi.org/10.1017/jfm.2013.498 Published online by Cambridge University Press

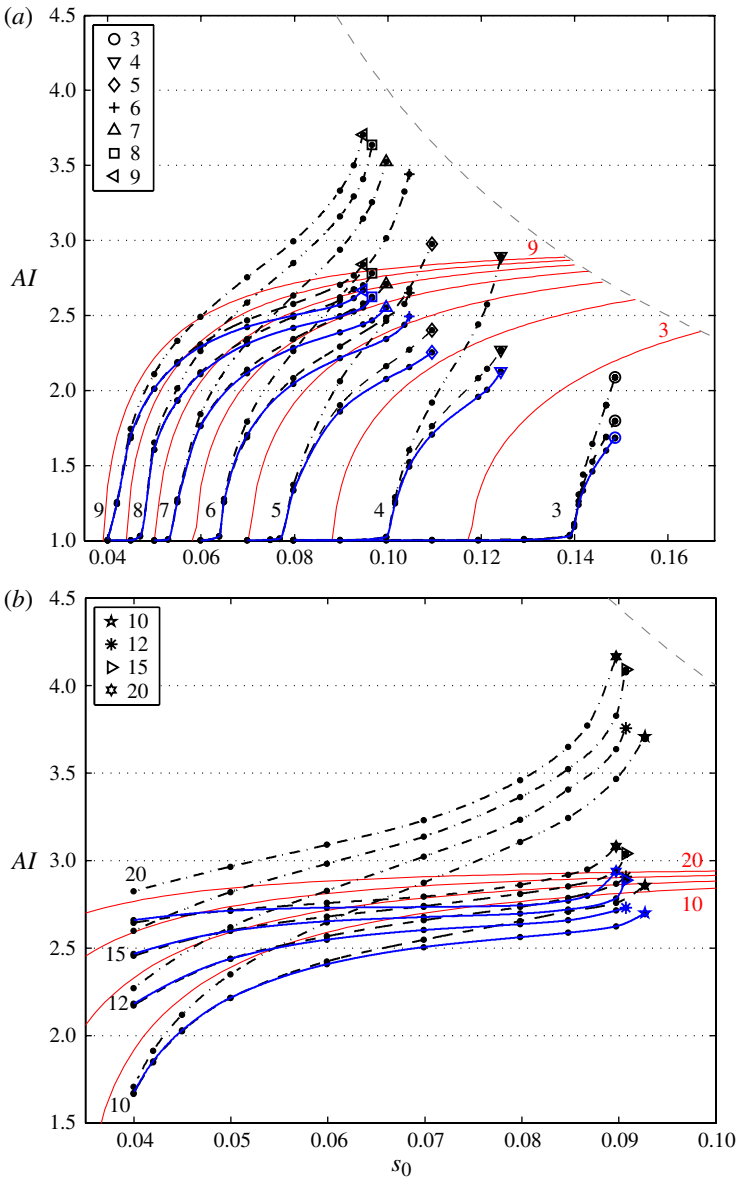


FIGURE 6. (Colour online) Symbols with lines show the amplification indices AI_{cr} (dash-dot), AI_{tr} (dashed) and AI_H (bold solid) as functions of steepness s_0 for different N_w (see values N_w in the legend, and numbers nearby the curves), obtained in the fully nonlinear simulations. The NLS envelope amplification AI_{env} (2.13) is shown by thin solid lines. The thin dashed curve, which cuts off the upper-right corner, corresponds to wave breaking condition $0.4/s_0$. Only the non-breaking cases are shown.

non-breaking cases figure 6(*a*,*b*) present dependencies of AI_{cr} (dash-dotted lines), AI_{tr} (thick dashed lines) and AI_H (bold solid lines) as functions of the initial wave steepness, s_0, for different N_w indicated in the legend by numbers. Figure 6(*a*) reports cases $N_w = 3, 4, 5, 6, 7, 9$ and figure 6(*b*) displays cases $N_w = 10, 12, 15, 20$. The

https://doi.org/10.1017/jfm.2013.498 Published online by Cambridge University Press

results of numerical simulations of wave amplification for wave groups comprising the same number of waves are shown by bold points and corresponding curves labelled with symbols at the ends, while thin solid curves plot the NLS amplification AI_{env} given by (2.13). The dashed thin curve $AI = 0.4/s_0$ cuts off the upper right corner in the figures, it roughly marks the condition of wave breaking. Note, that the actual steepness, s, does not differ much from the reduced one, s_0, for moderate steepness; for example, $s = 0.15$ corresponds to $s_0 \approx 0.1486$.

The most conspicuous feature of the amplification pattern is that some breathers do not grow at all despite the NLS prediction of growth for the same wave parameters. For example, three-wave modulations start to grow only for $s \gtrsim 0.142$, which is a noticeably steeper basic wave than follows from the weakly nonlinear theory, see figure 6(*a*). This agrees with earlier observations by Longuet-Higgins (1978) that the NLS prediction tends to underestimate the threshold of the BF instability; Henderson *et al.* (1999) did not observe regimes when three-wave modulations grew. Thus, overall the curves $AI(s_0)$ behave qualitatively similar to the prediction of the NLS theory; in particular, longer modulations result in greater wave enhancement. However, quantitatively the maximal amplifications might differ substantially from the weakly nonlinear theory prediction even for a quite moderate steepness; such an example is shown in figure 5(*a*).

According to figure 6, the height amplification AI_H is always less than the trough amplification AI_{tr}, which in turn, is always smaller than the crest amplification, AI_{cr}. While the trough amplification, AI_{tr}, is rather similar to the height amplification, AI_H, the crest amplification, AI_{cr}, is the most pronounced. The latter well exceeds the value of four, while the maximal through amplification is just above three. At the same time, the maximal wave height amplification is smaller than three. Note that three-wave modulations produce wave trains which could satisfy the rogue wave criterion only with respect to the wave crest $AI_{cr} > 2$; the two other amplification indices, AI_{tr} and AI_H, never exceed the threshold of two.

It is the onset of wave breaking that primarily limits the wave amplification for a given length of modulation. Owing to breaking the initially steep waves do not exhibit significant amplification. Breaking or near-breaking is observed starting with the initial wave steepness just above $s = 0.9$ for a long wave train of 20 waves. Although in contrast to Henderson *et al.* (1999), unstable behaviour of three-wave groups has been observed, for other values of N_w the domains of breaking and non-breaking cases in the parameter plane (s, N_w) seem to be consistent with results by Henderson *et al.* (1999), where modulations of up to 15 wavelengths were considered.

4.2. *Breaking and almost breaking waves*

The wave crest amplification curves from figure 6(*a*,*b*) are enlarged in figure 7; the picture is supplemented by the results of simulations identified as cases of wave breaking and by simulations for $N_w = 7/2$. The breaking cases are shown by crosses. Ensemble of 10 wave trains of Stokes waves with different phases, as shown in figure 18, is simulated for each breaking case. Evolution of such different realizations may result in rather different maximal wave amplification. Solid lines in figure 7 show the maximal wave amplification attained in all non-breaking and breaking cases for given N_w and wave steepness. The observed boundary of wave breaking regime agrees reasonably well with the thin dashed curve $AI_{cr} = 0.4/s_0$. It is important to note that the curves of wave amplification rise sharply once the wave is close to breaking. Therefore the near-breaking cases are expected to provide the most extreme waves. The behaviour of AI_{tr} and AI_H exhibits a similar pattern.

https://doi.org/10.1017/jfm.2013.498 Published online by Cambridge University Press

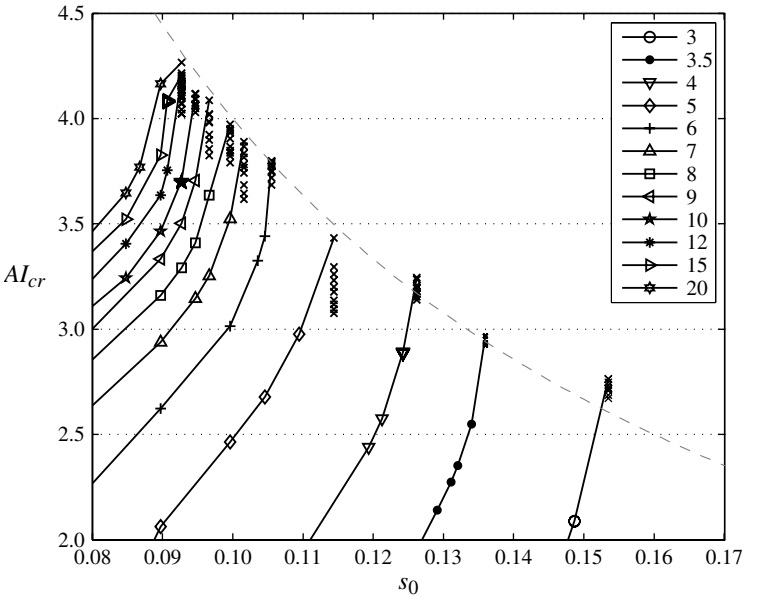


FIGURE 7. Zoomed wave crest amplification diagram shown in figure 6. Non-breaking cases are shown by symbols linked by solid lines, the breaking cases are shown by crosses. The thin dashed curve corresponds to $AI_{cr} = 0.4/s_0$.

Waves with the maximal crests, i.e. those which attain maximal AI_{cr}, exhibit noticeable front-back asymmetry. Their slope asymmetry is analysed in figure 8. Rear and front crest-steepness is shown in figure 8(*a*) and (*b*), respectively. The steepness is defined through the zero-crossing analysis of the wave crest. If H_{cr} is the wave crest height, and L_{zero}^{rear} and L_{zero}^{front} are, respectively, the horizontal distances between the coordinate of wave crest and the coordinates of zero-crossing of the backward and forward slopes, then the corresponding steepnesses are introduced as $s_{cr}^{rear} = \pi H_{cr}/(2L_{zero}^{rear})$ and $s_{cr}^{front} = \pi H_{cr}/(2L_{zero}^{front})$. In the limit of weak nonlinearity these steepnesses coincide with $s = k_0 H/2$; see dashed lines in figure 8 corresponding to the condition $s_{cr} = s_0$. Non-breaking cases are given by symbols, see the legend, while the cases identified as breaking ones are shown by crosses.

Figure 8 demonstrates that the front slopes of the maximal crest waves, s_{cr}^{front}, are noticeably steeper than the rear fronts. Wave breaking affects the front steepness more than the rear slope. The breaking limit does not show any dependence on the initial conditions and seems to be completely controlled by the wave crest steepness. The limiting steepness when waves start to break is roughly estimated according to figure 8 as $s_{cr}^{rear} \approx 0.5$ and $s_{cr}^{front} \approx 0.7$.

4.3. *Time of focusing and rogue wave lifetime*

The simulations also enable us to make conclusions about two characteristics important in the context of rogue waves: time of rogue wave formation and its lifetime. The conclusion is that the time of rogue wave formation or the time of fully nonlinear wave focusing is longer than that predicted by the NLS equation, see examples in figures 4 and 5. Focusing times are shown in figure 9(*a*) for the fully nonlinear simulations and in figure 9(*b*) for the NLS equation. Cases which are identified as

https://doi.org/10.1017/jfm.2013.498 Published online by Cambridge University Press

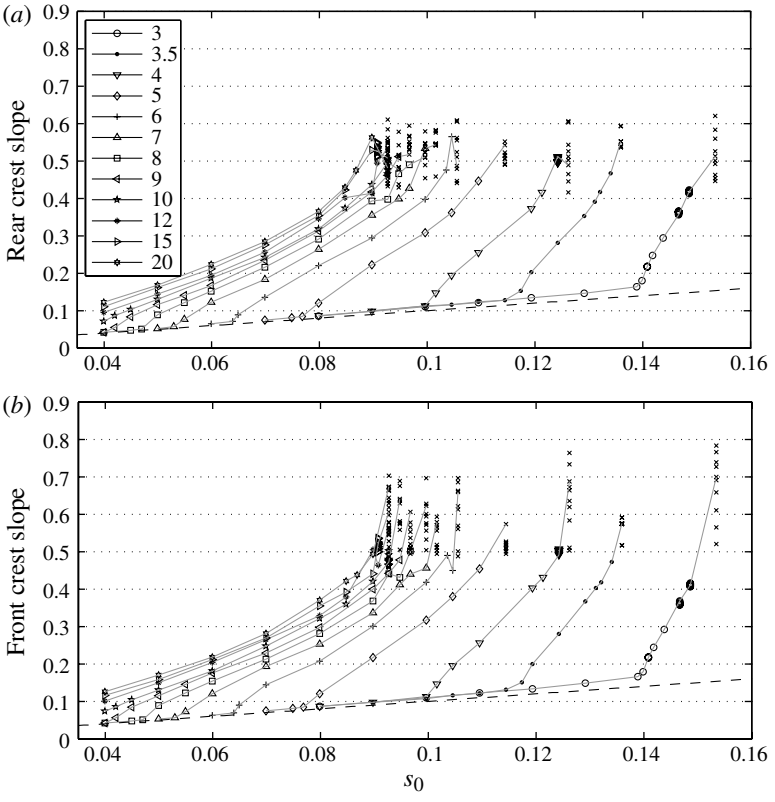


FIGURE 8. Steepness of the highest crest wave as a function of the initial wave steepness, s_0: (*a*) for rear crest slopes, s_{cr}^{rear}; (*b*) for front crest slopes, s_{cr}^{front}. Symbols show the results of numerical simulations for different N_w (see legend) with non-breaking waves. Crosses indicate breaking cases. Spots of densely spaced or overlapping symbols (see cases $N_w = 3$ and $N_w = 4$) correspond to situations, where to be certain whether breaking occurs or not the same envelopes were simulated 10 times for Stokes wave trains differing only in phase (as shown in figure 18). Solid lines link the data corresponding to the maximal crests. The dashed line indicates condition $s_{cr} = s_0$.

breaking or near-breaking, are shown by small crosses on solid lines in figure 9(*a*) in contrast to symbols which denote non-breaking situations.

The fastest growing breathers found in the fully nonlinear simulations correspond to $N_w = 3$ and $N_w = 4$ and $s \approx 0.15$ and $s \approx 0.125$, respectively, they attain the maximal modulation in $\sim$150 wave periods and overturn. Non-breaking cases need longer time to focus. The longest focusing found in the simulations is for the case $N_w = 9$ with $s = 0.042$, the time of focusing exceeds $2500T_0$, and is beyond the axis limit in figure 9(*a*). This condition corresponds to the case, when the wave steepness just slightly exceeds the modulational instability threshold. The NLS prediction of the focusing time (2.26) is shown in figure 9(*b*) for a realistic range of steepness of amplified waves, the same as shown in figure 6. The prediction of the NLS theory is qualitatively similar, but it noticeably underestimates the time of focusing. Obviously, the focusing time will decrease for stronger initial modulations, Δ. A rough estimate of this dependence is provided by the weakly nonlinear formula (2.26).

https://doi.org/10.1017/jfm.2013.498 Published online by Cambridge University Press

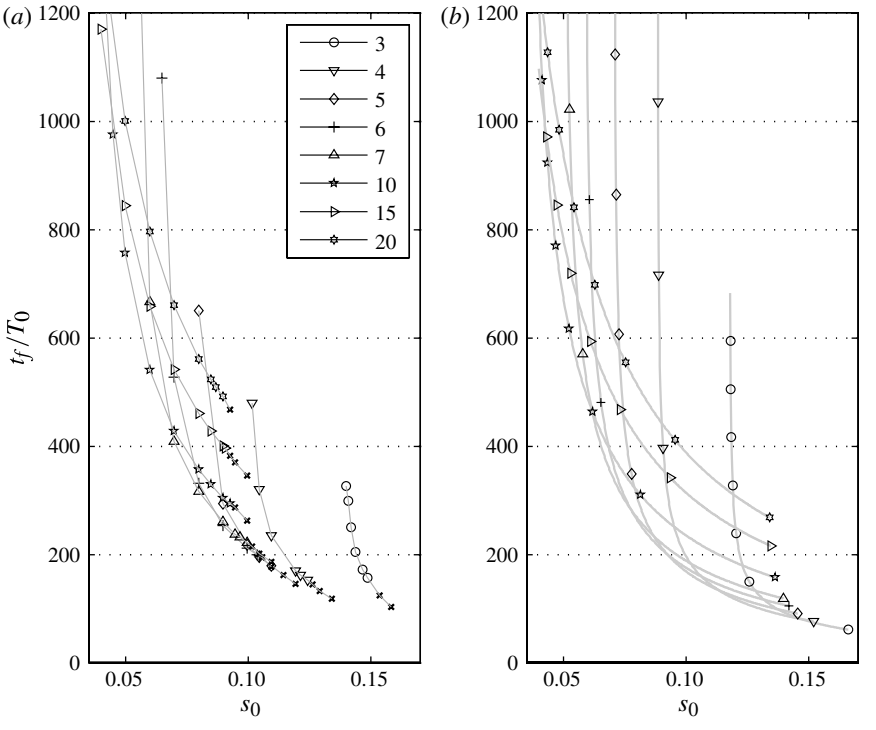


FIGURE 9. Focusing time as function of steepness s_0 for different N_w: (*a*) observed in the fully nonlinear simulations (symbols for non-breaking and small crosses for breaking cases); (*b*) the NLS prediction.

The lifetime of rogue waves observed in the fully nonlinear simulations of breathers is computed as the time interval when the maximal elevation of a wave group exceeds twice the initial amplitude, i.e. when $AI_{cr} > 2$. The values of the lifetime are shown in figure 10(*a*) as functions of s_0 for different N_w. The weakly nonlinear solution provided by (2.15) is shown in figure 10(*b*) for comparison.

Very good agreement is observed between figure 10(*a*) and (*b*); some quantitative discrepancy may be caused by somewhat different definitions of the lifetime, introduced using AI_{cr} or AI_{env}, respectively. Note, that sufficiently long modulations may produce very long-lived rogue waves satisfying the condition $AI_{cr} > 2$ for hundreds of wave periods. On the other hand, wave breaking which is more likely for long modulations results in considerable decrease of the rogue event lifetime.

4.4. *One-to-one mapping between the NLS and the fully nonlinear breathers*

This section addresses the question of how to link quantitatively the obtained results of the strongly nonlinear wave amplification to the weakly nonlinear NLS solutions. In this section we deal only with the results displayed in figure 6, as it describes the feature in which we are most interested, the maximal wave amplification.

We have noted earlier that the threshold of the modulational instability is underestimated in the weakly nonlinear framework, which is in agreement with Longuet-Higgins (1978). On the basis of our simulation we can estimate quantitatively the threshold steepness s_0^*, when the chosen wave modulation starts to grow, for cases $N_w = 3, 3.5, 4, 5, 6, 7, 8, 9$; see figure 6(*a*). It turns out that the same condition

https://doi.org/10.1017/jfm.2013.498 Published online by Cambridge University Press

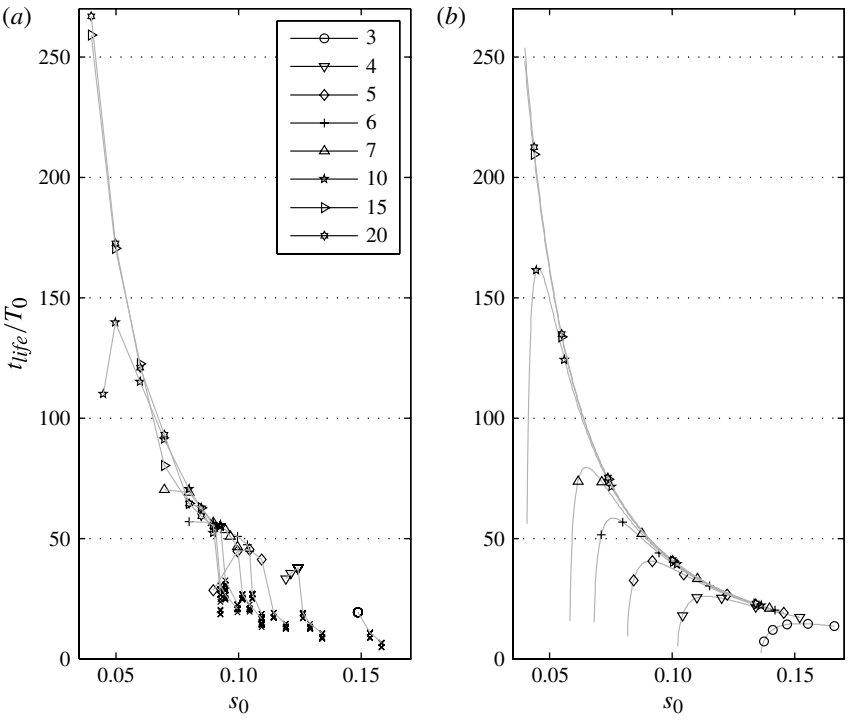


FIGURE 10. Rogue wave lifetime: (*a*) observed in the fully nonlinear simulations (symbols for non-breaking and crosses for breaking cases; criterion $AI_{cr} > 2$ is used); (*b*) the NLS prediction (criterion $AI_{env} > 2$ is used) as a function of steepness s_0 for different N_w (see the legend).

of instability formulated in terms of R_{BF}:$R_{BF} > 1$, can be extended for the strongly nonlinear cases just by redefining the parameter R_{BF}:

$$R_{BF}^{(fit)} = 2\sqrt{2}s_0(N_w - N_{adj}), \tag{4.4}$$

(cf. with (2.5)) where N_{adj} is a constant set equal to $N_{adj} = 0.47$. When the instability criterion is expressed in terms of the number of waves in one modulation, $N_w > N_w^*$, where $N_w^* \equiv N_{adj} + 2^{-3/2}(s_0^*)^{-1}$, then we have a simple good estimate of the threshold value of N_w^*. The relative error grows with N_w from less than 0.5 % for $N_w = 3$ to less than 6 % for $N_w = 9$. Thus, the modified single parameter $R_{BF}^{(fit)}$ (4.4) seems to work rather well within the range of examined initial wave steepnesses 0.04–0.14 (see figure 6).

It is obvious from figure 6 that the difference in amplification factors between the NLS and the primitive equations framework is substantial. However, since, crucially, the breather-like patterns survive in the full equations, an improved asymptotic description may be developed, which will make the calculations somewhat less elegant, but still straightforward. The discrepancy between the fully nonlinear simulations and the NLS framework is caused by a combination of the following effects:

(i) violation of the narrow-band approximation since wave groups become very short in the course of evolution;

https://doi.org/10.1017/jfm.2013.498 Published online by Cambridge University Press

(ii) high-order nonlinear interactions start to play an important role when waves become steep;

(iii) phase-locked bound wave components contribute greatly to the wave shape.

The importance of each of the above groups of effects is not *a priori* clear. The effects of the first group may be to a large extent captured by generalizations of the NLS equation such as the Dysthe-type equations (Dysthe 1979; Trulsen & Dysthe 1996). The effects of the second and the third kind can be in principle described with the help of a high-order asymptotic approach, if the increasing nonlinearity does not destroy the convergency of the expansions. We assume hereby that the wave envelope still may be introduced, although we do not discuss a specific recipe of how to do it. Hence, the problem can be split into two parts: (*a*) a description of the envelope evolution and (*b*) a description of the bound wave component.

An improvement in description of the envelope evolution could be obtained through modification of the evolution equation. Higher-order NLS generalizations for water waves lose the key property of integrability, which makes an analytic advance problematic. Corrections to weakly nonlinear weakly modulated waves due to bound harmonics are known in analytic forms up to the third order (see Dysthe 1979; Trulsen & Dysthe 1996; Slunyaev 2005). The dynamic of wave fields with wide spectra is governed by the Zakharov equations, and more complicated integral transformations should be employed to obtain the bound harmonics. There are analytic expressions for bound harmonics up to fourth order in steepness (Krasitskii 1994), but the formulae are notoriously bulky and are more suitable for numerics (see, e.g., Annenkov & Shrira 2013). In a particular degenerate case when the modulation is totally neglected, the wave field becomes a Stokes wave; then the Fourier amplitudes are expressed in power series of the wave amplitude; high-order asymptotic expansions for the Stokes waves are known in analytic form (see appendix C). Thus, the high-order Stokes wave representation is rather straightforward for applications.

Within the NLS framework it is natural to consider the effects of nonlinearity and dispersion to be of same order, $O(s) = O(\partial/\partial(k_0 x))$. At the maximum of the envelope the first derivative $\partial q/\partial x$ should be small (and $\partial|q|/\partial x = 0$), which suggests that the local effects in the vicinity of the maximum of the envelope might be captured in the first approximation by the expansion for uniform Stokes wave. Obtaining the bound wave corrections in such a way that we completely disregard the shape of the envelope, and specify amplitudes of the wave crest, A_{cr}, and wave trough, A_{tr}, as functions of the envelope amplitude, a_0,

$$s_{cr} = H_{Stokes}(s_0), \quad s_{cr} \equiv k_0 A_{cr}, \tag{4.5a}$$

$$s_{tr} = -H_{Stokes}(-s_0), \quad s_{tr} \equiv k_0 A_{tr}, \tag{4.5b}$$

where $s_0 \equiv k_0 a_0$. Here the function H_{Stokes} is based on the ninth-order Stokes wave expansion (see Lautrup 2011) as described in appendix C.

For a wave train of N_w waves and initial steepness s_0, also known as the non-dimensional amplitude of the envelope, the NLS equation predicts modulational growth of steepness up to $s^{(foc)} = s_0 AI_{env}$ with a known AI_{env}. Then the maximal amplitudes of the wave crest and wave trough can be expressed through the amplitude of the envelope $s^{(foc)}$ as

$$s_{cr}^{(foc)} = H_{Stokes}(s^{(foc)}), \quad s_{tr}^{(foc)} = -H_{Stokes}(-s^{(foc)}). \tag{4.6}$$

Then the wave crest and wave trough amplifications may be estimated as $s_{cr}^{(foc)}/s_{cr}$ and $s_{tr}^{(foc)}/s_{tr}$, respectively. These amplification factors can be improved compared with the

https://doi.org/10.1017/jfm.2013.498 Published online by Cambridge University Press

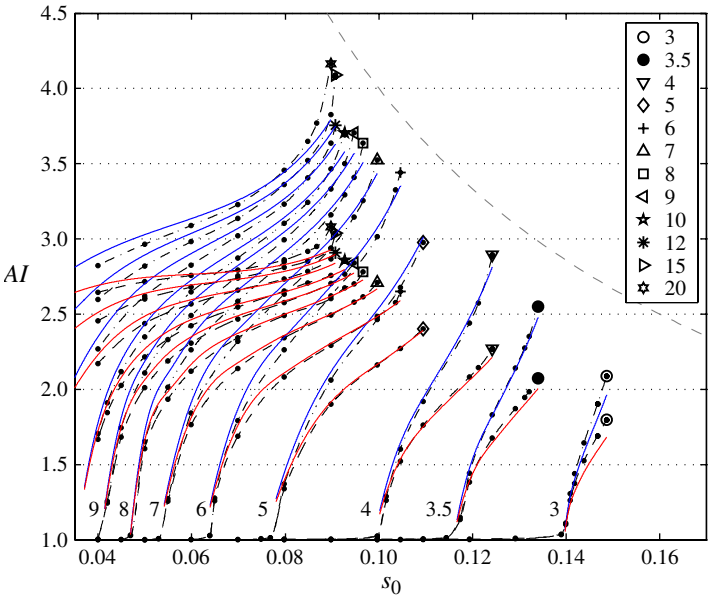


FIGURE 11. (Colour online) Wave crest and wave trough amplifications: least-squares fit of simple parametrization of the results of fully nonlinear simulations. The simulations are shown by bold points linked by dashed (AI_{tr}) and dash-dotted (AI_{cr}) lines. The analytic parametrization (4.7) is shown by solid lines.

NLS theory by taking into account the phase-locked Stokes wave components which capture the difference between wave crests and wave troughs. The results much more resemble the fully nonlinear simulations shown in figure 6 than the uncorrected NLS equation. However, to achieve quantitative agreement we have to improve AI_{env} as well.

Strongly nonlinear solutions for the wave envelope dynamics are unknown; we just know that the evolution is controlled by two independent parameters, s_0 and N_w. We make a bold assumption by looking for an improved envelope amplification formula for AI_{env} in the following form

$$AI_{env}^{(fit)} = AI_{env}\left[1 + \alpha(AI_{env})^{\beta}\right], \tag{4.7a}$$

$$AI_{cr}^{(fit)} = \frac{H_{Stokes}(s_0 AI_{env}^{(fit)})}{H_{Stokes}(s_0)}, \quad AI_{tr}^{(fit)} = \frac{H_{Stokes}(-s_0 AI_{env}^{(fit)})}{H_{Stokes}(-s_0)}. \tag{4.7b}$$

The fitting parameters, constants $\alpha = 1000$ and $\beta = 7$, are found by using an iterative procedure based upon the least-squares fit between the results of fully nonlinear simulations and ansatz (4.7); the result is shown in figure 11 and the fitting procedure is outlined below.

In figure 11 the description of amplifications of wave crests and wave troughs provided by fitting (4.7) shown by solid lines is compared with the results of fully nonlinear simulations shown by bold points. The bold points from the results with the breaking cases excluded are complemented by interpolating curves: dashed lines show AI_{tr}, while dash-dotted lines represent AI_{cr}. Cases with N_w from 3 to 20 are considered; the labelling symbols are shown at the end of the curves and in the legend.

https://doi.org/10.1017/jfm.2013.498 Published online by Cambridge University Press

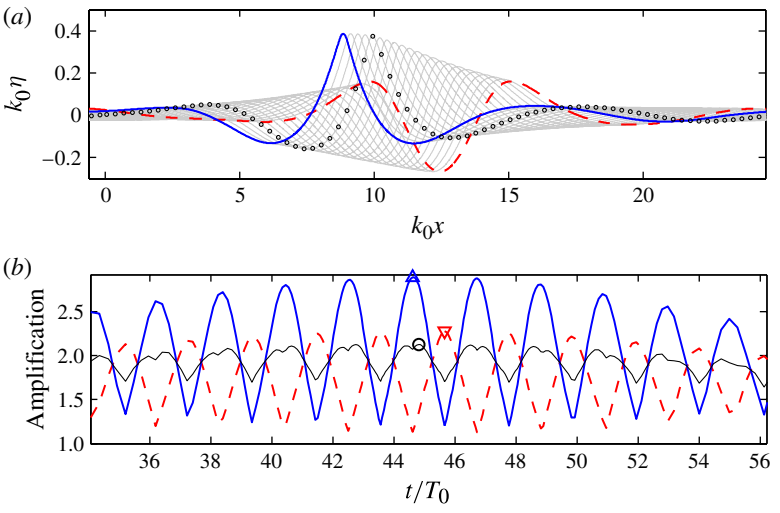


FIGURE 12. (Colour online) (*a*) Shapes of maximal waves and (*b*) the temporal evolution of amplification indices for the case $s = 0.125$, $N_w = 4$ and $\Delta = 0.01$: thick solid line, wave with the maximal crest; dashed line, wave with the deepest trough; circles in (*a*) and thin solid line in (*b*), wave with maximum trough-to-crest height. Symbols in (*b*) indicate the moments of maximal values for AI_{cr}, AI_{tr} and AI_H.

The initial condition for the optimization procedure was $\alpha = 0$, $\beta = 1$. Then, minimization of the mean square deviation between the data values and the fitted curves was performed by an iterative process; wave crest and wave trough amplifications were given equal weight. The outliers in fully nonlinear simulations, up to three points, corresponding to the most extreme amplification near the wave breaking onset were not taken into account in the fitting procedure. Finally the coefficients α and β were rounded off preserving the achieved quality of fitting: the resulting mean square root relative error for AI_{cr} and AI_{tr} does not exceed 15 %.

As attested by figure 11, the fitting based on a single parameter, λ or R_{BF}, proved to be surprisingly good in providing an analytic estimate of the strongly nonlinear numerical results. The discrepancy becomes noticeable only for very steep near-breaking waves with the maximal amplification ($N_w = 15, 20$); then the fitted function (4.7) is unable to capture accurately the actual dependence.

5. The maximal wave in a group

In this section we discuss the most amplified waves in more detail. Here, as well as in other parts of the work, we focus our attention onto non-breaking waves. Although the maximal wave crest amplification and the wave trough amplification well exceed the value of three, the wave trough-to-crest height remains below three in all non-breaking cases (figure 6). The train of 20 waves ($s = 0.93$ and $N_w = 20$), identified as a breaking case, results in a wave height amplification just slightly higher than three.

Surface elevation shapes of the maximally amplified waves are shown in figure 12(*a*) for $s = 0.125$ and $N_w = 4$ (the entire computational domain is shown). Evolution of amplification indices as functions of time is plotted in figure 12(*b*). The displayed case corresponds to almost breaking waves. The maximal values of the wave crest, trough and height amplifications are attained at close but different moments; they

https://doi.org/10.1017/jfm.2013.498 Published online by Cambridge University Press

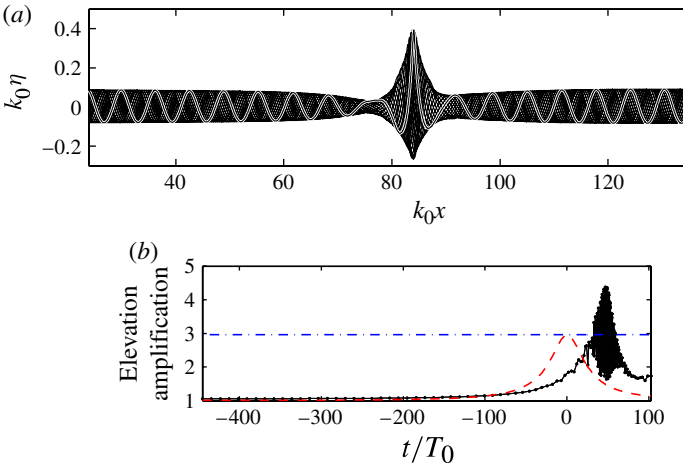


FIGURE 13. (Colour online) (*a*) Wave with the maximal crest and its envelope: a sequence of surface elevations within one wave period around the moment of the maximal wave crest (contrast line) is plotted in the reference frame moving with linear wave group speed. (*b*) Evolution of the wave crest amplification, AI_{cr}, for $s = 0.09$, $N_w = 20$ and $\Delta = 0.01$ is shown by dots connected by grey lines, the corresponding AI_{env} of the analytic breather solution is plotted by the dashed line.

are indicated by symbols in figure 12(*b*), the corresponding surface elevations are displayed in figure 12(*a*) by solid, dashed lines and by circles. Evolution of the surface shape is shown by the sequence of grey profiles. It follows from figure 12(*b*), that the wave crests and wave troughs are much more variable than AI_H, but oscillate only once within two wave periods. Function AI_H has two local maxima during two wave periods, these maxima coincide with neither the moment of the maximal wave crest amplification, AI_{cr}, nor the moment of the deepest trough, AI_{tr}. Essential for understanding this is the shortness of the wave group: the wave trough-to-crest height is strongly affected by the wave group envelope shape. This explains the much less enhanced wave heights in figure 6 compared with amplifications of wave crests and wave troughs. The wave train in figure 12(*a*) initially consists of four waves and is rather steep. The extreme waves shown in figure 12(*a*) are very steep and confined within a very short wave packet, less than a couple of wavelengths, while the wave field outside the group is quite small.

Remarkably, the picture of emerging extreme waves does not change noticeably if a much longer train is considered. To illustrate this point figure 13(*a*) shows the most amplified waves for the train of 20 waves and initial steepness $ka = 0.09$. The contrasting pale line shows the wave with the maximal crest amplification; it has large steepness and is close to overturning, it belongs to a very short asymmetric wave group. It looks very similar to the maximal crest wave in a much shorter wave train in figure 12(*a*). The waves outside the group have much smaller amplitude. We do not show the evolution of amplification ratio; it is also very similar to figure 12(*b*).

There is no standard way of introducing an envelope for strongly nonlinear short wave trains once they are no longer narrow-band; to make the envelope shape graphically evident a sequence of surface elevations is plotted in figure 13(*a*) in the frame moving with the linear wave group velocity C_g during one wave period around the moment of maximum wave crest.

https://doi.org/10.1017/jfm.2013.498 Published online by Cambridge University Press

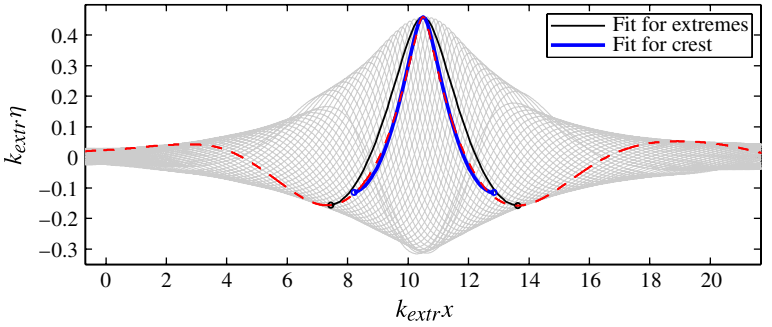


FIGURE 14. (Colour online) Wave with the maximal crest (dashed line), the envelope (grey lines, in the reference frame moving with velocity C_g) and fitted Stokes waves are shown for $s = 0.125$, $N_w = 4$ and $\Delta = 0.01$ (cf. figure 12, but note different scaling in comparison with figure 12); $k_0 = 4$ rad m^{-1}. Parameters of the fitted Stokes waves: $k_{extr} \approx 4.7$ rad m^{-1}, $k_{extr}H/2 \approx 0.31$, $k_{extr}\Delta\overline{\eta} \approx +0.1$ (thick line) and $s_{cr} \approx 0.39$ (thin solid line).

According to the NLS breather solution the modulation tends to zero outside the intense wave group, see (2.14) and figure 2; this feature is well observed in figure 13(*a*), although the envelope never decreases down to zero. Dependence of AI_{cr} on time is shown in figure 13(*b*) by a solid line with points and compared with the NLS prediction indicated by dashed line. The maximal amplification is ≈4.16, against 2.96 predicted by the NLS equation for the envelope (the dash-dotted curve).

We can also conclude that in the range of parameters for which the simulations were carried out, the maximally amplified wave train has very similar appearance regardless of the length of modulation and initial steepness. We stress that we are speaking about the universality of both the individual wave shape and the wave group envelope. The universality of extreme wave shape shown in figures 12(*a*) and 13(*a*) could be attributed to the fact that these waves are optimal with respect to maximal amplification of non-breaking modulated waves.

The shape of the maximal crest wave for $s = 0.125$ and $N_w = 4$ is considered in more detail in figure 14. Hereafter we focus on the wave attaining the maximal crest height. A sequence of surface elevations within one wave period in the comoving reference frame is shown by grey lines. It is natural to compare the shape of this maximal crest wave shown by a broken line with the shape of a uniform Stokes wave. To this end the Stokes wave is fitted to the maximum wave in two different manners.

In the first approach the points of the maximal crest and the troughs next to the maximal crest wave profile determine the length and height of the fitted Stokes wave. The Stokes wave fitted in such a way is shown by a thin solid line in figure 14. Initially, the carrier wavenumber is $N_w = 4$, while the maximal crest wave is noticeably shorter, $k_{extr} \approx 4.7$. This value of wavenumber is used to scale the axes in figure 14. Steepness understood as $k_{extr}H/2 \approx 0.31$ is not very high, but, as is easy to see from figure 14, the actual shape of the focused wave is significantly steeper than that of the Stokes wave fitted in such a way. Note, that there is also a significant mean water-level set-up: $k_{extr}\Delta\overline{\eta} \approx +0.1$, where $\Delta\overline{\eta}$ is the mean level elevation. This suggests that even a half wavelength is too large a scale to approximate the maximal crest wave, and an approach focused upon a more narrow vicinity of the crest would be better. An alternative approach is to employ the least-squares fit for the maximal wave crest. Thereby we estimate the wave crest steepness in terms of the uniform Stokes wave;

https://doi.org/10.1017/jfm.2013.498 Published online by Cambridge University Press

the fitted Stokes wave is shown in figure 14 by a thick solid line. The Stokes wave fitted in such a way describes very well the upper part of the maximal crest wave (the dashed line which shows the actual wave shape and the fitted curve coincide), although a discrepancy is apparent at the bottom. The fitted wave is shorter than the maximal wave and its steepness, $s_{cr} \approx 0.38$, is significantly higher than the estimate provided by the first approach.

For a wave with parameters $s = 0.09$ and $N_w = 20$, figure 13 exhibits a very similar picture. In this case the fitted Stokes wave is characterized by $k_{extr}H/2 \approx 0.31$, $k_{extr} \approx 24.0$ and $k_{extr}\Delta\overline{\eta} \approx +0.1$, the Stokes wave fitted to the maximum wave crest has steepness $s_{cr} \approx 0.41$.

In all simulations the maximal crest waves exhibit a quite noticeable increase of wavenumber, $k_{extr}/k_0 \approx 1.15 \ldots 1.25$. A less apparent feature of such waves is that the longer wavelength sidebands in the spectrum get more energy than the shorter-scale sidebands. Note that the $N_w = 20$ initial modulation exhibits only 19 wave crests in figure 13(*a*) and that the wave crest to the left from the maximal wave is flattened. The length of the maximal waves, in contrast, is shorter than the initial carrier wavelength; hence, the extreme wave groups are very inhomogeneous with strongly varying local wavenumber.

Front–back asymmetry of the maximal crest wave requires a brief discussion. Figure 8 shows front and rear wave crest slopes having rather different steepness, and the front slope is noticeably steeper. On the other hand, the wave asymmetry defined as the ratio

$$2(L^{front}_{trough} - L^{rear}_{trough})/(L^{front}_{trough} + L^{rear}_{trough}), \tag{5.1}$$

does not show a clear wave asymmetry for all non-breaking cases. Here L^{front}_{trough} and L^{rear}_{trough} are the horizontal distances from the wave crest to the front and rear troughs correspondingly, these three points mark the wave extremes, see figure 14. Analysis of maximal local steepness found as spatial derivative of the surface elevation shape, $s_{loc} \equiv \partial\eta/\partial x$, does not reveal any difference between positive and negative steepest slopes in non-breaking cases either. Thus, often the front–back asymmetry is not well manifested: it is difficult to discern it by unaided eye in figures 12(*a*), 13(*a*) and 14. It becomes more apparent for steeper and breaking waves. Overall, the issue of front–back asymmetry goes beyond the scope of this work, but it is important and requires a dedicated study.

Summarizing the properties of the maximal crest wave we reiterate the key finding: the maximally amplified wave train has very similar appearance regardless of the length of initial modulation and initial steepness, we even use the term ‘universal behaviour’. The maximal wave is noticeably shorter than the surrounding waves and belongs to a short group. The maximal wave is steeper than the Stokes wave with a similar length and height, it exhibits a noticeable set-up. The maximum wave crest locally may be well approximated by a steeper Stokes wave. The front slope of the wave crest is even steeper than the rear slope, and the front trough is then effectively longer than the rear trough. The maximum local wave slope s_{loc} in the simulations with waves close to breaking has values in the range 0.5–0.6.

6. Discussion of generality and robustness of breather dynamics

Breather-like wave groups were reported in a number of numerical (e.g. Henderson *et al.* 1999; Clamond *et al.* 2006) and laboratory (Karjanto & van Groesen 2010; Chabchoub, Hoffmann & Akhmediev 2011; Chabchoub *et al.* 2012*a*,*b*; Clauss *et al.*

https://doi.org/10.1017/jfm.2013.498 Published online by Cambridge University Press

2012; Shemer & Alperovich 2013) studies. The limiting case of a very steep and short wave group propagating over zero-magnitude background was also observed in numerical and laboratory experiments (Dyachenko & Zakharov 2008; Slunyaev 2009; Slunyaev *et al.* 2013*a*). Proximity of breather-like groups within the extended NLS equations to the solutions of the integrable NLS equation was shown in Schober (2006). Hence, there is no doubt that objects similar to breather wave groups do occur in reality, at least in the controlled reality of narrow laboratory tanks.

In the present study we considered and analysed the evolution of a fully nonlinear analogue of the NLS breather under the initial conditions most favourable for the growth of a single unstable mode. We established a clear one-to-one correspondence between the NLS and fully nonlinear breathers. However, while within the integrable NLS framework the role of breathers is established as absolutely fundamental, the place of their fully nonlinear counterparts in the large picture is not clear. The first key open questions one encounters when attempting to link the results to reality are how robust and how representative are the results? Below we try to address these questions by considering two factors which are the most likely to affect the wave field evolution: perturbations of the initial condition and the co-existence of several unstable modes.

6.1. *Effect of noisy perturbation of the initial conditions*

The weakly nonlinear initial condition used in the fully nonlinear simulations were designed to produce a single unstable mode, a fully nonlinear counterpart of the NLS breather. However, inevitably other unstable modes also become excited in the simulations. In all simulations discussed in this paper, the first 'breath' was controlled by the prescribed initial modulation, although after the moment of the first peak other uncontrolled effects become apparent; the field evolution becomes chaotic with time. The detailed analysis of this problem is complicated and goes beyond the scope of the paper, although the broad-brush picture is rather straightforward. Noisy perturbations withdraw a part of the energy from the primary unstable mode, which may result in several nonlinear modes competing in the processes of emergence of a pronounced group, especially if a faster growing unstable mode is excited. This picture is supported by the fully nonlinear simulations described below.

Revisit the example considered in § 3.3 illustrated by figures 17, 18 and 5, that is a plane Stokes wave of initial steepness $s = 0.09$ slightly modulated initially with the scale $N_w = 9$ and relative amplitude of modulation $\Delta = 0.01$. The ensuing evolution of the single-mode perturbation initiated in such a way is shown in figure 5. According to (2.7) and (2.6) for the unperturbed Stokes wave of the chosen steepness $s = 0.09$ the most unstable are shorter six-wave modulations. Since the prescribed perturbation, $N_w = 9$, is longer than the most unstable one, $N_w = 6$, it should lead to a stronger wave amplification according to relations (2.13) and (2.12) and (2.5), and also figure 6(*a*), but it takes a longer time to grow. According to figure 9(*a*) focusing times for fully nonlinear simulations with the same initial perturbation amplitude $\Delta = 0.01$ for modulations $N_w = \{5, 6, 7, 8, 9\}$ are $t_f \approx \{294, 255, 259, 273, 290\}T_0$, respectively. Thus, the six-wave modulation is the fastest in the fully nonlinear problem as well. This is a rather typical example: usually the greatest amplification is attained by the longest modulation although the corresponding growth rates are much smaller than those of the most unstable modes. Thus, there are natural general questions as follows. Are the patterns resulting from the prescribed dominant perturbation robust? Can the large amplitudes attained by long-wave perturbation in our sterile environment occur in a more noisy reality?

https://doi.org/10.1017/jfm.2013.498 Published online by Cambridge University Press

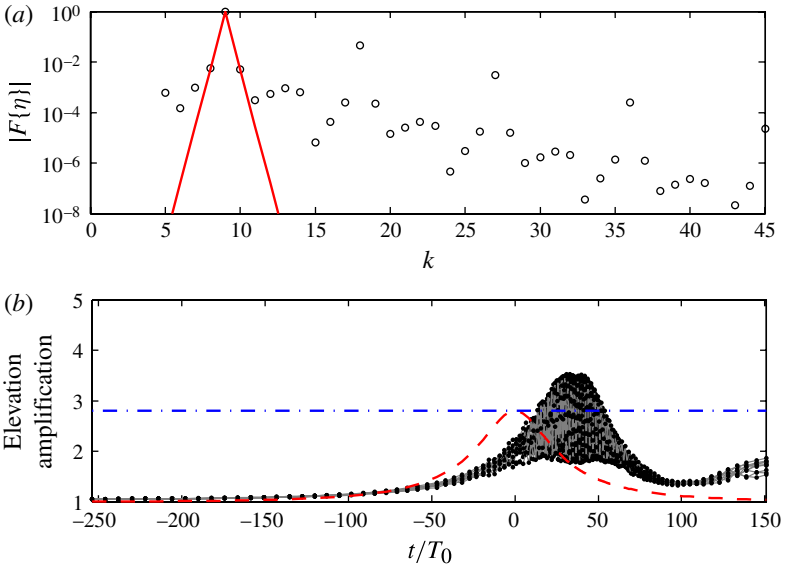


FIGURE 15. (Colour online) Fully nonlinear simulation of a breather with noisy perturbations of the initial modulation ($s = 0.09$, $N_w = 9$, $\Delta = 0.01$, $\Delta^{noise} = 0.001$): Fourier spectrum of the initial surface elevation (a) and evolution of the wave crest amplification in the fully nonlinear simulation (points linked by solid lines) and the weakly nonlinear solution (dashed line) (b) (cf. Figure 5). Five realizations of random noise perturbations are simulated and shown in (b).

To address these questions a series of simulations were carried out with the initial wave modulation weakly perturbed in a random way. The applied perturbation affects only the wave modulation, i.e. only non-zero Fourier components of q_{mod} are perturbed, see appendix B. Random perturbation amplitudes were chosen not to exceed a certain Δ^{noise} portion of the dominant wave amplitude, similar to definition of Δ, see (2.25). An example of the Fourier spectrum of the initial surface elevation for the case $s = 0.09$, $N_w = 9$ and $\Delta = 0.01$ is shown in figure 15(a). For a certainty, the initial levels of noisy perturbations are chosen to be 10 % of the initial magnitude of the prescribed dominant perturbation, that is $\Delta^{noise} = 0.1\Delta$. Although the two nearest sidebands in the initial condition seem to be specified exactly in accordance with the analytic formula, they experience a 10 % perturbation as well. *A priori* one might expect one of two possible outcomes: (i) the earlier studied solution is robust, the effect of noise is negligible in the time interval until the maximum of modulation is attained; (ii) two or more modes become dominant and the evolution becomes qualitatively different from the single-mode evolution scenarios considered so far. The scenario (i) is illustrated in figure 15 for $N_w = 9$. Under this scenario the primary nine-wave modulation, although not the fastest growing, does not suffer much from the introduced perturbation with a larger growth rate as can be easily seen by comparing figures 15(b) and 5(a); the field evolution nearly repeats the dynamics without the extra perturbation. Dependencies for five different realizations of irregular initial wave modulation perturbations are displayed in figure 15(b).

As could be expected, the 20-wave modulation with a low growth rate whose focusing time without noise, $t_f \approx 492T_0$, see figure 13(b) is much more sensitive to noise and the second scenario occurs. We do not illustrate it here. The highest

https://doi.org/10.1017/jfm.2013.498 Published online by Cambridge University Press

waves may develop significantly faster than without the noise even when the level of noisy perturbations is chosen even lower than previously. Crucially, the highest waves which occur, are of considerably smaller amplitude than they would have been without the noise. In this situation more than one unstable mode is excited; their interaction dramatically complicates the dynamics.

An obvious alternative way to increase robustness of the single breather regimes is to increase the amplitude of the prescribed dominant initial modulation, so far only a 1 % initial modulation was considered, which is rather small and much less than a typical experimental error bar in laboratory wave flumes. An increase of Δ generally leads to a better agreement with the NLS theory.

6.2. *Interaction of unstable modes*

The co-existence and interaction of several unstable modes is not uncommon, it significantly affects extreme wave formation. The interaction of nonlinear wave groups dramatically enriches wave dynamics: it may decrease or increase the maximal wave height. An excellent prototype example of a possible mechanism of significant increase is provided in the NLS context by high-order Peregrine breathers (see Akhmediev *et al.* 2009). These exact NLS solutions result in wave amplifications of 5, 7, 9, etc., times, compared with 3 for a single mode. These waves are not purely mathematical toys, they have been recently observed in wave flumes by Chabchoub *et al.* (2012*a*,*b*) (see the corresponding numerical simulations in Slunyaev *et al.* (2013*b*)). However, what is the maximal wave in a group resulting from the interaction of several breathers is not known beyond the NLS framework, the issue certainly needs a dedicated study. Here we consider just an example of such an interaction in order to illustrate certain affinity with the single-mode evolution. We simulate a second-order rational breather by means of the HOSM code. The NLS second-order rational breather solution is infinite in space; in order to fit the numerical solution to the periodic domain, the wave train is truncated in a smooth fashion far from the location of the initial perturbation, see figure 16(*a*). The modulation of the exact NLS solution $\pm|q(x)|$ is shown by dashed lines, and the initial wave elevation for the simulation is plotted by the solid line. The elevation and the surface velocity potential are computed from known $q(x)$ according to the third-order asymptotic reconstruction formulas (see Trulsen 2006). The initial condition is set at $\sim$200 wave periods prior to the time of maximal wave amplification.

The temporal dependence of the wave crest amplification with respect to the maximal wave elevation at $t \to -\infty$ is plotted in figure 16(*b*): the dashed line shows the analytic solution, and the solid line with points presents the results of simulations. In the weakly nonlinear theory the amplification factor should be five, while it exceeds six in the presented example of strongly nonlinear simulation. The simulated case is close to the onset of breaking, although the initial steepness is small. Compared with the NLS prediction a noticeable delay of the peak wave amplification is observed, similar to simulations of single breathers.

The wave with maximal crest elevation and the corresponding envelope is presented in figure 16(*c*). Comparing figures 16(*c*) and 13(*a*), one may conclude that the wave patterns exhibit remarkable similarities. The maximal crest wave profiles, shown by contrast lines, have very high and steep crests with untypically long front and rear troughs. The next crest, i.e. of the wave just behind the maximal crest wave and shown to the left, is strongly flattened, similar to the case in figure 13(*a*). The maximal crest wave groups are of similar height and length. On the other hand, the overall appearance of the envelope in figure 16(*c*) is more complicated. The maximal crest

https://doi.org/10.1017/jfm.2013.498 Published online by Cambridge University Press

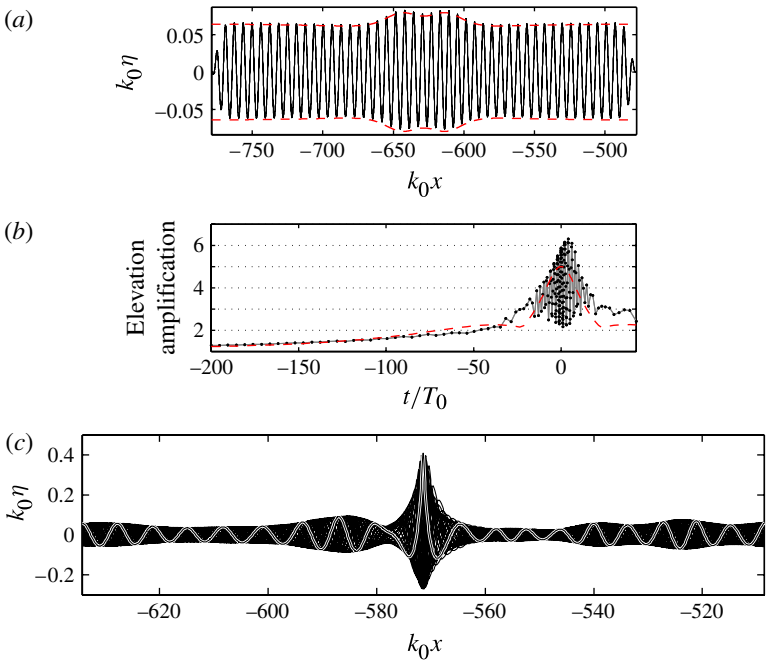


FIGURE 16. (Colour online) Simulation of the second-order rational breather solution with initial steepness $s_0 = 0.065$: (*a*) the initial surface elevation (solid line) and the exact analytic solution for wave envelope $\pm|q(x)|$ (dashed line); (*b*) temporal dependence of the maximum wave elevation, simulated (solid line with dots) and the analytic solution (dashed line); and (*c*) the wave with the highest crest elevation. In (*c*) a sequence of surface elevations within one wave period around the moment of the maximal crest (contrast line) is plotted in the frame of reference moving with linear wave group speed, C_g; this sequence of elevations provides the envelope.

group is no longer isolated, it certainly interacts with another intense wave group to the left of the main group.

Stokes wave profiles are fitted into the maximal crest wave shape in a similar way as in § 5, see figure 14. The obtained Stokes wave characteristics are pretty similar to those in the one-breather evolution cases, $k_{extr}H/2 \approx 0.31$, $k_{extr}/k_0 \approx 1.2$, $k_{extr}\Delta\overline{\eta} \approx +0.1$ and the fit to the wave crest gives estimation $s_{cr} \approx 0.43$. These simulations support the idea of universality of the maximal crest wave, the local shape and key parameters of the maximal crest wave prove to be very similar, independently of the way the maximal crest wave is created.

7. Concluding remarks

Here we first summarize the results of the paper and then very briefly discuss them from the perspective of developing short-term deterministic forecasting of rogue waves in the ocean. The present work examines properties of extreme water waves developing as a result of the BF instability of initially uniform slightly modulated wave trains. The consideration within the framework of the full Euler equations is confined to strictly two-dimensional non-breaking potential waves in deep water. We address the most basic questions about the extreme wave patterns possible for the chosen initial conditions. More specifically, we find what is the maximal possible

https://doi.org/10.1017/jfm.2013.498 Published online by Cambridge University Press

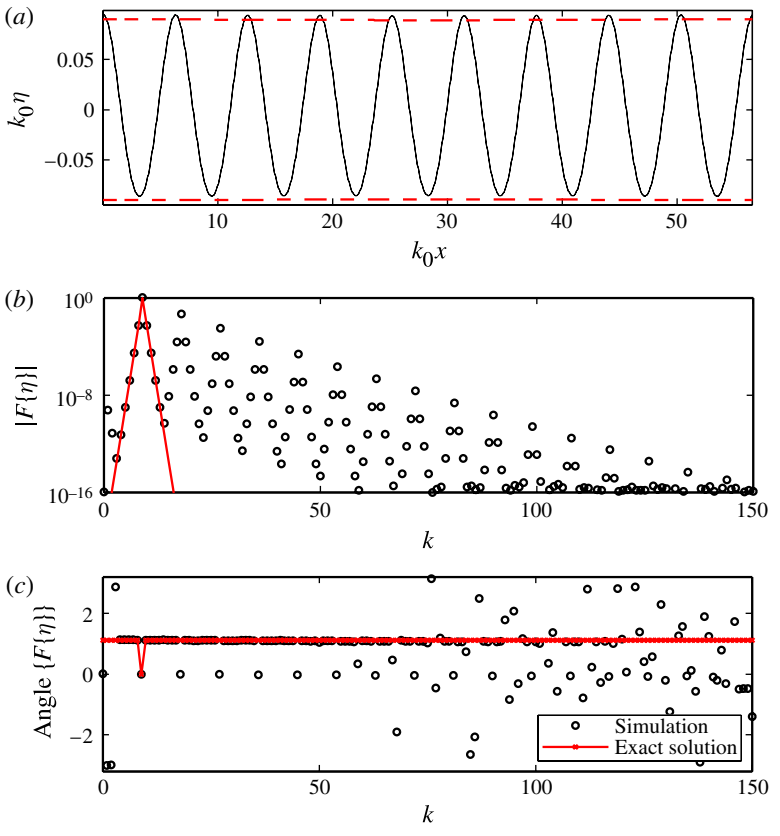


FIGURE 17. (Colour online) Initial condition for the case $s = 0.09$, $N_w = 9$ and $\Delta = 0.01$: (*a*) the surface elevation (solid line) and the envelope $\pm|q(x)|$ (dashed lines); (*b*) scaled Fourier spectrum for the elevation (circles) and the analytic breather solution (solid lines); (*c*) complex phases (in the range $(-\pi, \pi)$) of the Fourier spectrum.

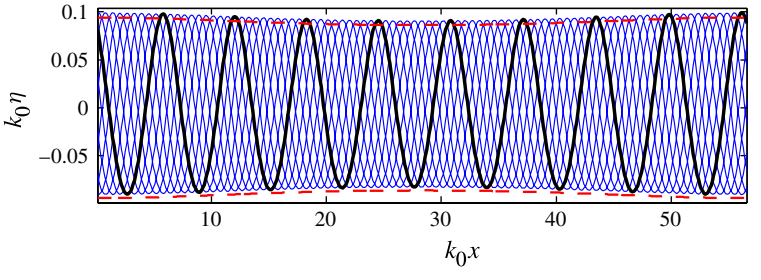


FIGURE 18. (Colour online) Ensemble of 10 shifted Stokes wave trains (solid lines) with the same modulation $\pm|q(x)|$ (dashed curves). The case $s = 0.09$, $N_w = 9$ and $\Delta = 0.1$ is shown.

non-breaking elevation, the deepest trough and the highest trough-to-crest height, what is the appearance of the extreme wave and the wave group it belongs to, what are the time scales of the extreme wave formation and its lifetime, and whether and how

https://doi.org/10.1017/jfm.2013.498 Published online by Cambridge University Press

the results of weakly nonlinear NLS theory can be applied for the description and forecasting of the dynamics of fully nonlinear waves.

The weakly nonlinear theory provided by the NLS equation serves as the reference point; within the NLS framework evolution of a single unstable mode is fully described by the breather solution of the NLS equation; crucially, interaction between unstable modes preserves the breathers intact. Evolution of a single unstable mode results in wave amplification not exceeding three times initial wave amplitude, the maximum occurs for the maximally long unstable modulation. Shorter modulations generally have higher growth rates, which results in a noticeably smaller wave enhancement. Whether the fully nonlinear counterparts of the NLS breathers exist in the primitive equations and, if they do, what their behaviour is was not entirely clear. By solving numerically the full Euler equations, we found that such isolated nonlinear patterns do exist, and their properties were examined to obtain a general picture of their evolution and to clarify the questions important in the context of rogue waves.

To create fully nonlinear counterparts to the NLS breathers, the initial conditions for fully nonlinear simulations are taken in the form of a train of Stokes waves modulated in accordance with the exact breather solution of the NLS equation. That is, the initial condition is the solution of the NLS equation, which corresponds to a chosen mode of the modulational instability; all bound wave components having Fourier amplitudes larger than the computer roundoff error are taken into account.

The ensuing modulational growth of steep waves is found to be weakened compared with the NLS theory: (i) for a chosen modulation wavelength the carrier wave amplitude threshold of instability is higher; (ii) the 'focusing time' increases, that is the time it takes for a weakly perturbed Stokes wave to attain the maximal amplification; (iii) the amplification of the wave trough-to-crest height in all simulations does not exceed the value of three. These results corroborate and extend the observations by Lighthill (1965) and Longuet-Higgins (1978), that BF instability growth rate is weaker in the fully nonlinear setting compared with the weakly nonlinear limit, while the instability domain shrinks (see Longuet-Higgins 1978, figures 7 and 9). Here we show that it takes a longer time for fully nonlinear breathers to attain their maximal amplitude than for their weakly nonlinear counterparts.

In contrast to the NLS theory, in situations with realistic wave train parameters, $N_w = 3$–20 and $s_0 = 0.04$–0.16, the maximal amplification of the wave crest and wave trough exceeds, respectively, four and three. The most substantial increase of the amplification occurs for near-breaking waves just prior to breaking. Since the employed models are not designed for the description of breaking waves, near-breaking wave dynamics requires further study. Unresolved wave breaking remains the major limitation of this study. On the qualitative level, the effect of breaking on wave dynamics, on the one hand, prevents wave amplification from exceeding a certain ceiling, which, counter-intuitively, results in smaller potential danger of initially steep waves: although such waves may grow more quickly, they break before attaining significant increase. On the other hand, we do not really know much about wave life after breaking: in some situations wave amplitude might continue to grow.

The very fact that the breather-like structures survive in the fully nonlinear simulations and behave qualitatively similar to the NLS framework, reveals that the underlying physics of the self-focusing effect remains qualitatively same. This gives us hope that improved theoretical models for wave modulations might lead to a reasonably good description of strongly nonlinear modulated waves. As an element of this strategy, the possibility of one-to-one mapping of weakly nonlinear breathers

https://doi.org/10.1017/jfm.2013.498 Published online by Cambridge University Press

having explicit analytic description to the results of fully nonlinear simulations has been demonstrated. We stress that in the present paper the term 'mapping' does not imply a rigourous one-to-one correspondence between all physical effects responsible for the modulation evolution in the original water equations and the NLS; our mapping is approximate and confined to the evolution of single breather patterns over the period not exceeding the cycle. A parametrization for the amplification factor based on the assumption of local validity of the high-order Stokes wave expansion provides a surprisingly good description of the wave crest and trough amplifications observed in simulations of even quite steep waves. A simple modification of the single controlling parameter R_{BF} is suggested to describe the onset of modulational growth in the strongly nonlinear case, which takes into account some wave decorrelation due to the strong nonlinearity. It tends to the standard definition (2.5) in the weakly nonlinear limit.

Lifetime is one of the key characteristics of rogue waves: the lifetime of fully nonlinear breathers proved to be well predicted by the NLS equation. Overall, the self-sustained soliton-like groups live longer than the linear ones, although the lifetime of a rogue wave modelled by a single breather does not differ significantly from that of a linear Gaussian wave group of similar length and amplitude.

Of special interest are the questions about the specific shape of the extreme waves and the wave groups they belong to. The most important observation in this context is the apparent 'universality' of the shape of the extreme wave and envelope, that is, the extreme wave with the highest crest for any given length of modulation is very similar regardless of the magnitude and wavelength of the initial single-mode perturbation. The extreme wave group with the maximal crest wave is always very short, it contains just about one-and-a-half waves, whatever the length of the initial modulation. Such groups are asymmetric; the local wavenumber is strongly inhomogeneous, see figures 12(*a*), 13(*a*), 14 and 16(*c*). Invariably, the maximal crest wave is shorter than the unperturbed carrier wave, its wavenumber k_{extr} is about $1.15–1.25k_0$, where k_0 is the wavenumber of the unperturbed Stokes wave. It is steeper than the Stokes wave of the same length and height due to a narrower crest, the top of the wave in the vicinity of the crest is similar to the limiting Stokes wave crest. The maximal wave crest has somewhat steeper front slope than the rear one. The discrepancy between the strong amplification for the maximal wave crest and a moderate one for the trough-to-crest height is essentially due to the shortness of the wave packet and the set-up localized within the packet: the packet length is comparable with wavelength; as a result the maximal wave experiences a rise of the order of $k_{extr}\Delta\overline{\eta} \approx 0.1$.

We stress that the extreme wave groups resulting from nonlinear focusing studied in the present paper are qualitatively different from groups of linear waves. We consider only the situations where the wave growth is due to nonlinear wave focusing, that is caused by deterministic coherent dynamics of the waves involved. These situations are particular cases of a strongly idealized two-dimensional 'sea' made mostly of breathers. In the NLS limit this model sea degenerates into soliton gas where patterns pass through each other. It is possible to consider random seas within the framework of such a model and then discuss the kinetics of breathers. We know the law of their interaction as is the case in the NLS limit. One can introduce energy spectra for the wave field and even consider realistic looking spectra, although it should be noted, the breather solution possesses its own specific spectrum shape which is not directly related to the spectrum of the sea state which it belongs to. However, under no circumstances will the kinetics of breathers tend to the classical weak turbulence kinetics where free waves interact with each other. There is no meaningful linear

https://doi.org/10.1017/jfm.2013.498 Published online by Cambridge University Press

limit either and, hence, no link to the theory of linear Gaussian fields. For wave fields with a substantial fraction of breathers the wave evolution cannot be considered as a stationary Gaussian random process even in the leading order, and the near-Gaussian 'quasi-deterministic' theory by Lindgren (1970) and Boccotti (1997) and its modifications do not apply.

Thus, within the classical fluid mechanics framework, we have clarified the basic questions about the extreme non-breaking waves that we posed; in this narrow sense, the problem has been solved. However, to apply the obtained results to the problem of real rogue waves in the ocean, one encounters a further layer of difficult questions which are beyond the scope of the present work. Nevertheless, it makes sense to outline these questions and where we are in resolving them, to see the gap to be overcome for deterministic forecasting of rogue waves in the ocean. The most obvious questions in need of a dedicated study are how robust the examined evolution scenarios of the breathers are and what their place in the big picture is. A preliminary study of emergence and evolution of breathers out of noisy initial conditions we have carried out in § 6.1 suggests certain robustness of the found regimes of evolution: if initially, for whatever reason, one unstable mode is excited, a moderate amount of noise in the initial moment is unlikely to affect noticeably the ensuing breather evolution. However, the very long modulations found to be the most dangerous in the artificially clean environment are much more susceptible to noise; shorter modulations emerging out of noise are more likely to prevail. Thus, it is not clear under what conditions the most dangerous long modulations might develop in the ocean. Nevertheless, even if the long modulations do not develop at all and shorter ones prevail, the found near-universal behaviour of the extreme wave and the envelope might still be relevant. A brief consideration of evolution of two interacting wave groups in § 6.2 supports this suggestion; see also a recent study of multibreathers by Slunyaev *et al.* (2013*b*). The extreme waves are found to be weakly dependent on whether they resulted from a single-mode modulation, long or short, or produced by the interaction of two unstable modes, the wave limiting configuration seems to be determined primarily by local effects. This conjecture is in line with the mechanism of incipient breaking due to superharmonic instabilities proposed by Longuet-Higgins & Cokelet (1978), Longuet-Higgins (1984) and Longuet-Higgins, Cleaver & Fox (1994) and later supported by observations reviewed in Babanin (2011). We have not considered what happens to the extreme wave after breaking. From observations we know that the waves often decrease their amplitude after breaking, but some waves might continue to grow with a breaker on the crest. The problem requires a dedicated study and there exist numerical tools which could handle such a problem even for three-dimensional waves (e.g. Biausser *et al.* 2004; Iafrati *et al.* 2012).

The three-dimensionality of real wave fields in the ocean is another major challenge. Very little is known about the dynamics of essentially three-dimensional strongly nonlinear wave patterns, although even in the three-dimensional setting the dominant instability remains two-dimensional for waves of steepness typical of oceanic conditions (e.g. McLean 1982; Stiassnie & Shemer 1984). There exist simulations of almost two-dimensional waves including breather-like waves in a fully nonlinear setting (Slunyaev *et al.* 2002; Slunyaev, Sergeeva & Pelinovsky 2012; Ruban 2011), which support robustness of the two-dimensional idealization in our context. There are also field observations suggesting that the pronounced wave groups are nearly two-dimensional (e.g. Nieto Borge, Reichert & Hessner 2013). However, to what extent such observations could justify the use of the two-dimensional simulations for rogue wave forecasting is unclear at the moment. Probably, if a pronounced quasi-

https://doi.org/10.1017/jfm.2013.498 Published online by Cambridge University Press

two-dimensional wave group is identified in real-time records, such a group could be reasonably well described by a two-dimensional breather and its subsequent evolution over a few tens of wave periods would be close to the scenarios outlined in the present work. It remains a challenging but achievable task to find out when and to what extent this guess is true.

Acknowledgements

The authors gratefully acknowledge support from the EC 7th Framework Programme (Grant PIIF-GA-2009-254389/909389) without which the work would have never happened. A.V.S. is grateful to colleagues in the Department of Mathematics and EPSAM at Keele for the warm hospitality. A.V.S. also acknowledges partial support from RFBR grants 11-02-00483 and 12-05-33087.

Appendix A. Numerical codes

A few simulations of the NLS equation are reported in this paper with the purpose of estimating the effect of discretization and numerical errors on the exact breather solution. A split-step-Fourier approach similar to that by Lo & Mei (1985) and a Runge–Kutta method are used to integrate the NLS equation. Short-scale filters are used to damp the high-frequency instabilities, when necessary.

To obtain the most reliable results, two numerical approaches for solving inviscid irrotational primitive equations of ideal hydrodynamics are employed: the fully nonlinear conformal mapping approach following Zakharov *et al.* (2002) and the strongly nonlinear HOSM (West *et al.* 1987). In this study, we used the version where up to seven-wave interactions are resolved ($M = 6$); a five-point spectral filter is used to suppress the short-scale instability. These codes have already been employed in other tests of strongly nonlinear dynamics of the NLS equation solutions (e.g. Slunyaev 2009; Slunyaev *et al.* 2012).

The governing equations comprise the Laplace equation, two surface boundary conditions and the bottom boundary condition,

$$\frac{\partial \eta}{\partial t} + \frac{\partial \phi}{\partial x}\frac{\partial \eta}{\partial x} = \frac{\partial \phi}{\partial z}, \quad z = \eta, \tag{A 1}$$

$$\frac{\partial \phi}{\partial t} + g\eta + \frac{1}{2}\left(\left(\frac{\partial \phi}{\partial x}\right)^2 + \left(\frac{\partial \phi}{\partial z}\right)^2\right) = 0, \quad z = \eta, \tag{A 2}$$

$$\frac{\partial^2 \phi}{\partial x^2} + \frac{\partial^2 \phi}{\partial z^2} = 0, \quad z \leqslant \eta, \tag{A 3}$$

$$\phi \to 0, \quad z \to -\infty. \tag{A 4}$$

Most of the simulations are performed by the solver of the potential Euler equations written in conformal variables (Zakharov *et al.* 2002), hereinafter it is refereed to as the fully nonlinear code. In this approach, the fluid volume is mapped to a half-plane with constant boundaries, and the system (A 1) and (A 2) is reduced to equations on the conformal variables. To initiate the simulation, the initial surface elevation, $\eta(x)$, and the surface velocity potential $\Phi(x) \equiv \phi(x, z = \eta(x))$ are required. The special feature of the simulations is our approach to choosing the initial conditions we discuss in appendix B.

The same fields, $\eta(x)$ and $\Phi(x)$, provide the initial condition for a simulation by the HOSM. Strictly speaking, the HOSM is not fully, but strongly nonlinear, since

https://doi.org/10.1017/jfm.2013.498 Published online by Cambridge University Press

it employs an asymptotic expansion of the velocity potential near the still water surface. However, for such a high order of the expansion, $M = 6$, which captures up to seven-wave nonlinear interactions, the method is known to be very close to the fully nonlinear solution (see the discussion in Clamond *et al.* 2006). In the simulations, very steep waves occur for a short duration, and thus it is reasonable to hope that errors due to the slow convergence of the expansion do not accumulate. Note that close to the moment when the HOSM blows up due to wave breaking, the wave shapes are found to be quite similar in the HOSM and the fully nonlinear simulations.

As a very steep wave may indeed develop during the simulations, the breaking may occur. Often, numerical codes become unstable in such a case, which manifests the breaking; the HOSM is an example. However, the employed fully nonlinear code in conformal variables is so stable that it may overpass the moment of breaking; then the breaking manifests itself in the change of the total wave energy in the computation domain. Since in numerical simulations there is always some energy leakage due to computer round-off, it is not evident how to recognize the physical onset of wave breaking. The evolution of the spectrum tail serves as a good indicator. Indeed, when the spectrum becomes too wide, the spectral resolution has to be increased to continue the simulations maintaining the proper accuracy and to approach the breaking limit. On approaching the breaking limit the required computational efforts are gradually increasing. However, we stress this point, our study does not aspire to describe accurately the breaking or almost breaking waves. In our simulations to describe a single wave we use 400 or less points in space. A wave is recognized as breaking or near breaking by tracing the behaviour of the total energy. The threshold of maximum total energy variation is set on the basis of comparative simulations of the same initial problems by means of the conformal mapping solution of the Euler equations and the HOSM.

As the HOSM blows up when waves start to overturn, this moment is assumed to correspond to the physical wave breaking. Thus, we set the threshold value of the energy error in the fully nonlinear simulation of the same problem. If the energy variation in another fully nonlinear simulation with similar initial conditions exceeds the chosen threshold value, the wave is labelled as breaking. Typically, this threshold corresponds to $\sim 0.01\,\%$ of the total energy variation. Thus, the accuracy of the simulations far exceeds the level reported by Tanaka (1990) and Henderson *et al.* (1999).

Appendix B. Initial conditions

To make a meaningful comparison of the NLS breather with fully nonlinear simulations, it is crucial to reproduce in the simulations the wave which corresponds to a single unstable mode. It is generally understood that such a mode represents a weakly modulated wave train long before the focusing time, $t \to -\infty$, turning into an intense wave group at the focusing moment. It is expected that at the focusing moment the assumptions underlying the NLS equation may be violated, while at $t \to -\infty$ we can choose a perturbation in such a way that the wave field is characterized by sufficient smallness of wave steepness and the narrow enough spectrum.

In the fully nonlinear simulations, to excite a single unstable mode, breather, the initial conditions far from the focusing moment are prescribed in the form of a weakly modulated Stokes wave. The Stokes wave is the stationary solution of the Euler equations; here it is found numerically with very high accuracy. The modulation is prescribed in accordance with the exact breather solution of the NLS equation bearing

https://doi.org/10.1017/jfm.2013.498 Published online by Cambridge University Press

in mind that it describes the free wave component, and hence bound waves should be modulated accordingly. The following five-step procedure is used to produce the initial conditions.

Step 1

The uniform train in the form of N_w consecutive Stokes waves of steepness $s \equiv k_0 H/2$ is prescribed in a periodic domain, in terms of the surface elevation and the surface velocity potential,

$$\eta_{Stokes}(x) \quad \text{and} \quad \Phi_{Stokes}(x). \tag{B 1}$$

This stationary solution is obtained by using a numerical high-order asymptotic procedure, which builds the Stokes wave fields in conformal variables. For the sake of simplicity we choose the size of the spatial domain to be equal to 2π in all cases and, correspondingly, the carrier wavenumber $k_0 \equiv N_w$.

Step 2

Complex wave fields are obtained employing the Hilbert transforms of the surface elevation $\tilde{\eta} = \hat{H}\{\eta\}$ and the surface velocity potential $\tilde{\Phi} = \hat{H}\{\Phi\}$. In the Fourier space the procedure works as follows

$$\hat{F}\{\tilde{\eta}\}_k = \begin{cases} 2\hat{F}\{\eta_{Stokes}\}_k & \text{if } k < 0 \\ 0 & \text{elsewhere,} \end{cases} \tag{B 2a}$$

$$\hat{F}\{\tilde{\Phi}\}_k = \begin{cases} 2\hat{F}\{\Phi_{Stokes}\}_k & \text{if } k < 0 \\ 0 & \text{elsewhere,} \end{cases} \tag{B 2b}$$

$$\tilde{\eta} = \hat{F}^{-1}\{\hat{F}\{\tilde{\eta}\}\}, \quad \tilde{\Phi} = \hat{F}^{-1}\{\hat{F}\{\tilde{\Phi}\}\}. \tag{B 2c}$$

Here $\hat{F}$ and $\hat{F}^{-1}$ are direct and inverse Fourier transform operators respectively.

Thus, $\tilde{\eta}$ and $\tilde{\Phi}$ are complex-valued functions which correspond to the fully nonlinear generalization of the complex amplitude $q(x)$. At the same time, the Hilbert envelopes $|\tilde{\eta}|$ and $|\tilde{\Phi}|$ are not the free-wave envelopes (they include a combination of free and bound waves). Functions $\pm|\tilde{\eta}|$ and $\pm|\tilde{\Phi}|$ are not the enveloping curves for $\eta(x)$ and $\Phi(x)$ either.

Step 3

The Fourier amplitude $|\hat{F}\{\tilde{\eta}\}_{k_0}|$ of the carrier wavenumber, $k_0 = N_w$, specifies the amplitude of the free-wave component, a_0, and the associated wave steepness, $s_0 \equiv N_w a_0$ and, hence, the eigenvalue λ by virtue of (2.12). Then, the focusing time, $t_f = 4T_f/\omega_0/s_0^2$, is estimated according to (2.26) for the chosen amplitude of wave perturbation, Δ, for the carrier wavenumber, N_w, and the wave steepness, s_0. Substitution of the found parameters into the exact NLS solution (2.10) provides the envelope shape q at time $-t_f$: $q(x, t = -t_f)$.

Step 4

In the Fourier space the carrier wave component is easily extracted from the envelope $q(x, t = -t_f)$, it corresponds to the wavenumber $k = 0$ of the Fourier transform of the envelope. Only the spectral sidebands within the range $-N_w/2 \cdots N_w/2$ are left, while

https://doi.org/10.1017/jfm.2013.498 Published online by Cambridge University Press

the other spectral components are put equal to zero,

$$\hat{F}\{q_{mod}\}_k = \begin{cases} \hat{F}\{q\}_k & \text{if } 0 < |k| < N_w/2 \\ 0 & \text{elsewhere,} \end{cases} \tag{B 3a}$$

$$q_{mod} = \hat{F}^{-1}\{\hat{F}\{q_{mod}\}\}. \tag{B 3b}$$

This truncation of the spectrum tails is made to avoid the overlap between sidebands of multiple harmonics of the modulated Stokes wave.

Step 5

Finally, the train of modulated Stokes waves we are looking for is obtained as real parts of the surface elevation and velocity fields multiplied by the modulation shape (cf. (2.4)),

$$\eta(x, t = -t_f) = \mathrm{Re}\{\tilde{\eta}(1 + q_{mod})\} \quad \text{and} \quad \Phi(x, t = -t_f) = \mathrm{Re}\{\tilde{\Phi}(1 + q_{mod})\}. \tag{B 4}$$

The result is illustrated in figure 17 for the example $s = 0.09$ and $N_w = 9$. In figure 17(*a*) the asymmetry of the surface elevation with respect to the symmetric envelope $\pm|q(x)|$ (dashed lines) is evident, while the modulation is so small that it cannot be noticed by eye. The corresponding Fourier spectrum is shown in figure 17(*b*) by circles, and the analytic NLS solution for the envelope spectrum is shown by solid lines. The dominant harmonic is at $k = N_w$, and many other Stokes harmonics are observed; they are modulated according to the free-wave part of the spectrum. The Fourier phases displayed in figure 17(*c*) show that the modulation has different phase with respect to the carrier Stokes wave; the phases start to deviate from the NLS solution when the magnitudes of the Fourier amplitudes come close to the computer roundoff limit. Plots of the surface velocity potential look quite similar. For the case shown in figure 17 the reduced steepness is $s_0 \approx 0.0897$, the eigenvalue is $\lambda \approx 0.8997$, and the focusing time due to the NLS estimation (2.26) is $t_f \approx 254T_0$, where $T_0 = 2\pi/\omega_0$ is the linear wave period.

For fixed normalized amplitude of perturbation Δ, there are two main parameters of the problem, the steepness of the unmodulated wave, s, and the modulation number, N_w. The third parameter appears when the phase difference between the carrier wave and the modulation is taken into account, i.e. the location of the maximal modulation with respect to the position of a wave crest. Solutions of the NLS equation are invariant with respect to this parameter. Owing to the difference between the phase and group velocities of deep-water waves, it is natural to expect this phase shift to have no significant effect on the results if the modulation is long or if the evolution of the envelope is slow with respect to wave period. The latter condition holds for most of the simulated cases.

However, when the modulation length is just a few wavelengths or the envelope evolves relatively fast, the particular position of the wave crest within the envelope may become important. Therefore, in situations of this kind a sequence of initial conditions, which have the same envelope modulation, but different phases between the carrier wave crests and the modulation, is simulated serially. An example of the sequence of initial wave shapes is shown in figure 18 for $s = 0.09$ and $N_w = 9$ by solid lines, where the modulation is unusually large, $\Delta = 0.1$, for the purpose of illustration. One of the waves is plotted by a thicker line. The dashed curves show the envelope $\pm|q(x)|$.

https://doi.org/10.1017/jfm.2013.498 Published online by Cambridge University Press

Appendix C. The ninth-order expansion for Stokes waves

Function H_{Stokes} is introduced to describe the Stokes wave using a high-order asymptotic expansion. Here we employ the ninth-order expansion for the Stokes wave (following Lautrup 2011).

The surface elevation $\eta(x)$ of a Stokes wave with the carrier wavenumber k_0 has the form

$$k_0\eta = \sum_{n=1}^{n=9} F_n \cos(nk_0x), \quad F_n(A) = \sum_{m=n}^{m=9} F_{nm}A^m, \tag{C 1}$$

where, in notation of this paper, A is equal to s_0, and then $H_{Stokes}(s) \equiv \sum_{n=1}^{n=9} F_n(s)$. Coefficients F_{nm} are given below:

$$F_{11} = 1, \quad F_{13} = \frac{9}{8}, \quad F_{15} = \frac{769}{192}, \quad F_{17} = \frac{201457}{9216}, \quad F_{19} = \frac{325514563}{2211840}, \tag{C 2a}$$

$$F_{22} = \frac{1}{2}, \quad F_{24} = \frac{11}{6}, \quad F_{26} = \frac{463}{48}, \quad F_{28} = \frac{1259}{20}, \tag{C 2b}$$

$$F_{33} = \frac{3}{8}, \quad F_{35} = \frac{315}{128}, \quad F_{37} = \frac{85563}{5120}, \quad F_{39} = \frac{5101251}{40960}, \tag{C 2c}$$

$$F_{44} = \frac{1}{3}, \quad F_{46} = \frac{577}{180}, \quad F_{48} = \frac{57703}{2160}, \tag{C 2d}$$

$$F_{55} = \frac{125}{384}, \quad F_{57} = \frac{38269}{9216}, \quad F_{59} = \frac{318219347}{7741440}, \tag{C 2e}$$

$$F_{66} = \frac{27}{80}, \quad F_{68} = \frac{30141}{5600}, \tag{C 2f}$$

$$F_{77} = \frac{16807}{46080}, \quad F_{79} = \frac{51557203}{7372800}, \tag{C 2g}$$

$$F_{88} = \frac{128}{315}, \tag{C 2h}$$

$$F_{99} = \frac{531441}{1146880}. \tag{C 2i}$$

REFERENCES

Ablowitz, M. J., Hammack, J., Henderson, D. & Schober, C. M. 2001 Long-time dynamics of the modulational instability of deep water waves. *Physica* D **152–153**, 416–433.

Ablowitz, M. J. & Herbst, B. M. 1990 On homoclinic structure and numerically induced chaos for the nonlinear Schrödinger equation. *SIAM J. Appl. Maths* **50**, 339–351.

Akhmediev, N. N. & Ankiewicz, A. 1997 *Solitons - Nonlinear Pulses and Beams*. Chapman & Hall.

Akhmediev, N., Ankiewicz, A. & Soto-Crespo, J. M. 2009 Rogue waves and rational solutions of the nonlinear Schrödinger equation. *Phys. Rev.* E **80**, 026601.

Akhmediev, N. N., Eleonskii, V. M. & Kulagin, N. E. 1987 Exact first-order solutions of the nonlinear Schrödinger equation. *Theor. Math. Phys. USSR* **72**, 809–818.

Annenkov, S. Y. & Shrira, V. I. 2013 Large-time evolution of statistical moments of wind wave fields. *J. Fluid Mech.* **726**, 517–546.

Babanin, A. 2011 *Breaking and Dissipation of Ocean Surface Waves*. Cambridge University Press.

Benjamin, T. B. & Feir, J. E. 1967 The disintegration of wavetrains in deep water. Part 1. *J. Fluid Mech.* **27**, 417–430.

https://doi.org/10.1017/jfm.2013.498 Published online by Cambridge University Press

BIAUSSER, B., FRAUNIE, P., GRILLI, S. & MARCER, R. 2004 Numerical analysis of the internal kinematics and dynamics of 3-D breaking waves on slopes. *Intl J. Offshore Polar Engng* **14**, 247–256.

BOCCOTTI, P. 1997 A general theory of three-dimensional wave groups. Part I: the formal derivation. *Ocean Engng* **24**, 265–280.

CHABCHOUB, A., HOFFMANN, N. P. & AKHMEDIEV, N 2011 Rogue wave observation in a water wave tank. *Phys. Rev. Lett.* **106**, 204502.

CHABCHOUB, A., HOFFMANN, N., ONORATO, M. & AKHMEDIEV, N. 2012*a* Super rogue waves: observation of a higher-order breather in water waves. *Phys. Rev.* X **2**, 011015.

CHABCHOUB, A., HOFFMANN, N., ONORATO, M., SLUNYAEV, A., SERGEEVA, A., PELINOVSKY, E. & AKHMEDIEV, N. 2012*b* Observation of a hierarchy of up to fifth-order rogue waves in a water tank. *Phys. Rev.* E **86**, 056601.

CLAMOND, D., FRANCIUS, M., GRUE, J. & KHARIF, C. 2006 Long time interaction of envelope solitons and freak wave formations. *Eur. J. Mech. (*B*/Fluids)* **25**, 536–553.

CLAUSS, G. F., KLEIN, M., DUDEK, M. & ONORATO, M. 2012 Application of breather solutions for the investigation of wave/structure interaction in high steep waves. *Proceedings of 31th International Conference on Ocean, Offshore and Arctic Engineering*, OMAE 83244-1–13.

CRAIK, A. D. D. 1985 *Wave Interactions and Fluid Flows*. Cambridge Monographs on Mechanics. Cambridge University Press.

DRAZIN, P. G. & JOHNSON, R. S. 1996 *Solitons: an Introduction*. Cambridge University Press.

DUBARD, P., GAILLARD, P., KLEIN, C. & MATVEEV, V. B. 2010 On multi-rogue wave solutions of the NLS equation and positon solutions of the KdV equation. *Eur. Phys. J. Special Topics* **185**, 247–258.

DYACHENKO, A. I. & ZAKHAROV, V. E. 2008 On the formation of freak waves on the surface of deep water. *J. Expl Theor. Phys. Lett.* **88**, 307–311.

DYSTHE, K. B. 1979 Note on a modification to the nonlinear Schrödinger equation for application to deep water waves. *Proc. R. Soc. Lond.* A **369**, 105–114.

DYSTHE, K., KROGSTAD, H. E. & MÜLLER, P. 2008 Oceanic rogue waves. *Annu. Rev. Fluid Mech.* **40**, 287–310.

DYSTHE, K. B. & TRULSEN, K. 1999 Note on breather type solutions of the NLS as models for freak-waves. *Phys. Scr.* T **82**, 48–52.

FENTON, J. D. 1985 A fifth-order Stokes theory for steady waves. *J. Waterways Port Coast. Ocean Engng* **111**, 216–234.

GAILLARD, P. 2012 Wronskian representation of solutions of the NLS equation and higher Peregrine breathers. *J. Math. Sci.: Adv. Appl.* **13**, 71–153.

HENDERSON, K. L., PEREGRINE, D. H. & DOLD, J. W. 1999 Unsteady water wave modulations: Fully nonlinear solutions and comparison with the nonlinear Schrödinger equation. *Wave Motion* **29**, 341–361.

IAFRATI, A., BABANIN, A. & ONORATO, M. Modulational instability, wave breaking and formation of large-scale dipoles in the atmosphere. Preprint (2012) arXiv: 1208.5392.

ISLAS, A. L. & SCHOBER, C. M. 2005 Predicting rogue waves in random oceanic sea states. *Phys. Fluids* **17**, 031701.

JANSSEN, P. 2004 *The Interaction of Surface Waves and Wind*. Cambridge University Press.

KARJANTO, N. & VAN GROESEN, E. 2010 Qualitative comparisons of experimental results on deterministic freak wave generation based on modulational instability. *J. Hydro-environ. Res.* **3**, 186–192.

KHARIF, C., PELINOVSKY, E. & SLUNYAEV, A. 2009 *Rogue Waves in the Ocean*. Springer.

KRASITSKII, V. P. 1994 On reduced equations in the Hamiltonian theory of weakly nonlinear surface waves. *J. Fluid Mech.* **272**, 1–20.

KUZNETSOV, E. A. 1977 Solitons in a parametrically unstable plasma. *Sov. Phys. Dokl.* **22**, 507–508.

LAUTRUP, B. 2011 Stokes waves. In *Physics of Continuous Matter, Second Edition: Exotic and Everyday Phenomena in the Macroscopic World*. CRC Press.

LIGHTHILL, M. J. 1965 Contribution to the theory of waves in nonlinear dispersive systems. *J. Inst. Maths Applics.* **1**, 269–306.

https://doi.org/10.1017/jfm.2013.498 Published online by Cambridge University Press

LINDGREN, G. 1970 Some properties of a normal process near a local maximum. *Ann. Math. Statist.* **4**, 1870–1883.

LO, E. & MEI, C. C. 1985 A numerical study of water-wave modulation based on a higher-order nonlinear Schrödinger equation. *J. Fluid Mech.* **150**, 395–416.

LONGUET-HIGGINS, M. S. 1975 Integral properties of periodic gravity waves of finite amplitude. *Proc. R. Soc. Lond.* A **342**, 157–174.

LONGUET-HIGGINS, M. S. 1978 The instabilities of gravity waves of finite amplitude in deep water. II. Subharmonics. *Proc. R. Soc. Lond.* A **360**, 489–505.

LONGUET-HIGGINS, M. S. 1984 On the stability of steep gravity waves. *Proc. R. Soc. Lond.* A **396**, 269–280.

LONGUET-HIGGINS, M. S., CLEAVER, R. P. & FOX, M. J. H. 1994 Crest instabilities of gravity waves. Part 2. Matching and asymptotic analysis. *J. Fluid Mech.* **259**, 333–344.

LONGUET-HIGGINS, M. S. & COKELET, E. D. 1978 The deformation of steep surface waves on water. II. Growth of normal-mode instabilities. *Proc. R. Soc. Lond.* A **364**, 1–28.

MCLEAN, J. W. 1982 Instabilities of finite-amplitude water waves. *J. Fluid Mech.* **114**, 315–330.

MICHELL, J. H. 1893 The highest waves in water. *Phil. Mag. Series 5* **36**, 430–437.

NEWELL, A. C. 1985 *Solitons in Mathematics and Physics*. Society for Industrial and Applied Mathematics.

NIETO BORGE, J. C., REICHERT, K. & HESSNER, K. 2013 Detection of spatio-temporal wave grouping properties by using temporal sequences of X-band radar images of the sea surface pH. *Ocean Model.* **61**, 21–37.

OLAGNON, M. & ATHANASSOULIS, G. A. (Eds) 2001 *Rogue Waves 2000*. Ifremer.

OLAGNON, M. & PREVOSTO, M. (Eds) 2005 *Rogue Waves 2004*. Ifremer.

OLAGNON, M. & PREVOSTO, M. (Eds) 2009 *Rogue Waves 2008*. Ifremer.

ONORATO, M., WASEDA, T., TOFFOLI, A., CAVALERI, L., GRAMSTAD, O., JANSSEN, P. A., KINOSHITA, T., MONBALIU, J., MORI, N., OSBORNE, A. R., SERIO, M., STANSBERG, C. T., TAMURA, H. & TRULSEN, K. 2009 Statistical properties of directional ocean waves: the role of the modulational instability in the formation of extreme events. *Phys. Rev. Lett.* **102**, 114502.

OSBORNE, A. R. 2010 *Nonlinear Ocean Waves and the Inverse Scattering Transform*, Int. Geophysics Ser., 97, Academic.

PEREGRINE, D. H. 1983 Water waves, nonlinear Schrodinger equations and their solutions. *J. Austral. Math. Soc. Ser.* B **25**, 16–43.

RUBAN, V. 2011 Enhanced rise of rogue waves in slant wave groups. *J. Expl Theor. Phys. Lett.* **94**, 194–198.

SCHOBER, C. M. 2006 Melnikov analysis and inverse spectral analysis of rogue waves in deep water. *Eur. J. Mech. (*B*/Fluids)* **25**, 602–620.

SCHOBER, C. M. & CALINI, A. 2008 Rogue waves in higher-order nonlinear Schrodinger models. In *Extreme Waves* (ed. E. Pelinovsky & C. Kharif), pp. 31–52. Springer.

SHEMER, L. & ALPEROVICH, L. 2013 Peregrine breather revisited. *Phys. Fluids* **25**, 051701.

SHRIRA, V. I. & GEOGJAEV, V. V. 2010 What makes the Peregrine soliton so special as a prototype of freak waves? *J. Engng Maths* **67**, 11–22.

SLUNYAEV, A. V. 2005 A high-order nonlinear envelope equation for gravity waves in finite-depth water. *J. Expl Theor. Phys.* **101**, 926–941.

SLUNYAEV, A. 2006 Nonlinear analysis and simulations of measured freak wave time series. *Eur. J. Mech. (*B*/Fluids)* **25**, 621–635.

SLUNYAEV, A. V. 2009 Numerical simulation of 'limiting' envelope solitons of gravity waves on deep water. *J. Expl Theor. Phys.* **109**, 676–686.

SLUNYAEV, A. 2010 Freak wave events and the wave phase coherence. *Eur. Phys. J. Special Topics* **185**, 67–80.

SLUNYAEV, A., CLAUSS, G. F., KLEIN, M. & ONORATO, M. 2013*a* Laboratory tests of short intense envelope solitons. *Phys. Fluids* **25**, 067105.

SLUNYAEV, A., KHARIF, C., PELINOVSKY, E. & TALIPOVA, T. 2002 Nonlinear wave focusing on water of finite depth. *Physica* D **173**, 77–96.

https://doi.org/10.1017/jfm.2013.498 Published online by Cambridge University Press

SLUNYAEV, A., PELINOVSKY, E., SERGEEVA, A., CHABCHOUB, A., HOFFMANN, N., ONORATO, M. & AKHMEDIEV, N. 2013*b* Super rogue waves in simulations based on weakly nonlinear and fully nonlinear hydrodynamic equations. *Phys. Rev.* E **88**, 012909.

SLUNYAEV, A. V., SERGEEVA, A. V. & PELINOVSKY, E. N. *et al.* 2012 Modelling of deep-water rogue waves: different frameworks. In *CENTEC Anniversary Book. Marine Technology and Engineering* (ed. C. Guedes Soares), pp. 199–216. Taylor & Francis Group.

STIASSNIE, M. & SHEMER, L. 1984 On modifications of the Zakharov equation for surface gravity waves. *J. Fluid Mech.* **143**, 47–67.

SONG, J.-B. & BANNER, M. L. 2002 On determining the onset and strength of breaking for deep water waves. Part I: unforced irrotational wave groups. *J. Phys. Oceanogr.* **32**, 2541–2558.

TANAKA, M. 1990 Maximum amplitude of modulated wavetrain. *Wave Motion* **12**, 559–568.

TRULSEN, K. 2006 Weakly nonlinear and stochastic properties of ocean wave fields: application to an extreme wave event. In *Waves in Geophysical Fluids: Tsunamis, Rogue Waves, Internal Waves and Internal Tides* (ed. J. Grue & K. Trulsen), CISM Courses and Lectures, 489, Springer.

TRULSEN, K. & DYSTHE, K. B. 1996 A modified nonlinear Schrödinger equation for broader bandwidth gravity waves on deep water. *Wave Motion* **24**, 281–289.

YUEN, H. C. & LAKE, B. M. 1982 Nonlinear dynamics of deep-water gravity waves. *Adv. Appl. Mech.* **22**, 67–327.

WEST, B. J., BRUECKNER, K. A., JANDA, R. S., MILDER, D. M. & MILTON, R. L. 1987 A new numerical method for surface hydrodynamics. *J. Geophys. Res.* **92**, 11803–11824.

WHITHAM, G. B. 1974 *Linear and Nonlinear Waves*. Wiley.

ZAKHAROV, V. 1968 Stability of periodic waves of finite amplitude on a surface of deep fluid. *J. Appl. Mech. Tech. Phys.* **2**, 190–194.

ZAKHAROV, V. E., DYACHENKO, A. I. & VASILYEV, O. A. 2002 New method for numerical simulation of a nonstationary potential flow of incompressible fluid with a free surface. *Eur. J. Mech. (*B*/Fluids)* **21**, 283–291.

ZAKHAROV, V. E. & OSTROVSKY, L. A. 2009 Modulation instability: the beginning. *Physica* D **238**, 540–548.

ZAKHAROV, V. E. & SHABAT, A. B. 1972 Exact theory of two-dimensional self-focusing and one-dimensional self-modulation of waves in nonlinear media. *Sov. Phys. JETP* **34**, 62–69.

https://doi.org/10.1017/jfm.2013.498 Published online by Cambridge University Press